2012

Electromagnetically induced transparency-based slow and stored light in warm atoms

Irina Novikova
William & Mary, inovikova@physics.wm.edu

Ronald L. Walsworth

Ronald L. Walsworth

Yanhong Xiao

Recommended Citation

Novikova, Irina; Walsworth, Ronald L.; Walsworth, Ronald L.; and Xiao, Yanhong, Electromagnetically induced transparency-based slow and stored light in warm atoms (2012). *Laser & Photonics Reviews*, 6(3), 333-353.
10.1002/lpor.201100021

Laser Photonics Rev. **6**, No. 3, 333–353 (2012) / **DOI** 10.1002/lpor.201100021

LASER & PHOTONICS REVIEWS

Abstract This paper reviews recent efforts to realize a high-efficiency memory for optical pulses using slow and stored light based on electromagnetically induced transparency (EIT) in ensembles of warm atoms in vapor cells. After a brief summary of basic continuous-wave and dynamic EIT properties, studies using weak classical signal pulses in optically dense coherent media are discussed, including optimization strategies for stored light efficiency and pulse-shape control, and modification of EIT and slow/stored light spectral properties due to atomic motion. Quantum memory demonstrations using both single photons and pulses of squeezed light are then reviewed. Finally a brief comparison with other approaches is presented.

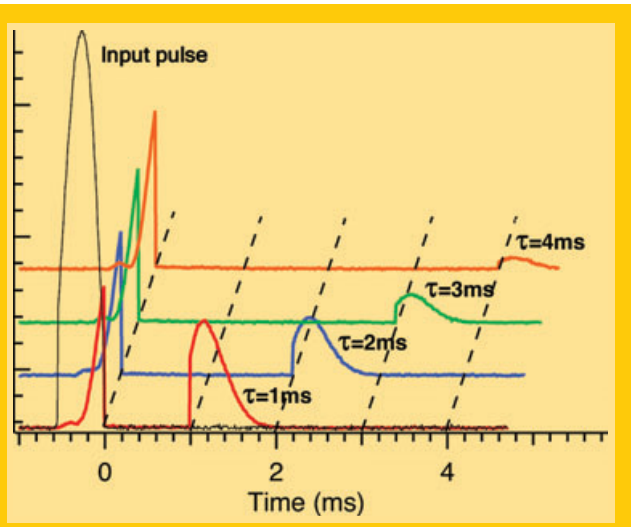

Electromagnetically induced transparency-based slow and stored light in warm atoms

Irina Novikova[1,*], Ronald L. Walsworth[2], and Yanhong Xiao[3]

1. Introduction

In recent years, an increasing number of applications, such as quantum information and quantum sensor technologies, have had their performance improved as a result of harnessing the quantum mechanical properties of light. Many of these applications rely on the ability to couple light to resonant systems, such as ensembles of atoms (warm or cold), "atom-like" defects in solid-state systems (such as nitrogen vacancy centers in diamond) or nanostructures (such as quantum dots), and photonic structures. A prominent example is electromagnetically induced transparency (EIT), which allows controlled manipulations of the optical properties of atomic or atom-like media via strong coupling of a near-resonant optical signal field and collective long-lived ensemble spin by means of a strong classical optical control field [1,2]. EIT has become a versatile tool for realization of controllable atom-light coupling, such as the manipulation of optical pulse propagation through atomic and atom-like media via slow [3–5] and stored light [6–9].

One of the exciting potential applications of EIT and slow and stored light is for practical realization of a quantum memory. This rapidly evolving area of research has been reviewed in several publications over the last decade [10–16]. In this review we focus on experiments aimed at optimizing EIT-based slow and stored light using warm atoms contained in vapor cells of various configurations. The key difference between cold and warm atomic ensembles is the thermal motion of warm atoms, which produces significant Doppler broadening of optical transitions. However, the broadening of the two-photon spin transition can be minimized by working in collinear geometry (e. g., co-propagating control and signal fields). The residual Doppler broadening caused by small mismatch of the wavelengths of the two fields can be practically eliminated by restriction of the motion of atoms in a region smaller than a microwave transition wavelength (e. g., by adding an inert buffer gas), thereby operating in a Dicke narrowing regime for the two-photon transition [17]. Thus, warm atomic ensembles can be as practical as cold atoms for coherent manipulations of atomic spins using EIT [7, 18–22]. In addition, warm-vapor-cell experiments have several attractive features, including relative simplicity of design and easy control over large atomic ensembles. A typical vapor cell is a sealed glass cylinder or sphere containing a small amount of solid metal (e. g., Rb or Cs). The atomic vapor concentration can be easily controlled by changing the temperature of the glass cell. Moreover, any unwanted external magnetic fields can be effectively eliminated by placing the atomic vapor cell in a high-permeability magnetic shielding enclosure. The interaction time of warm atoms with EIT laser fields is extendable to several milliseconds by introducing an inert buffer gas at a pressure of a few torr into the vapor cell to restrict the motion of alkali metal atoms to slow diffusion, or by employing an

[1] College of William & Mary, Williamsburg, VA 23187, USA [2] Harvard-Smithsonian Center for Astrophysics and Harvard University, Cambridge, MA 02138, USA [3] Fudan University, Shanghai 200433, China
[*] Corresponding author: e-mail: inovikova@physics.wm.edu

anti-relaxation wall coating on the inner surface of the vapor cell. In addition, recent progress in chip-scale atomic clocks [23] and magnetometers [24] employing EIT and related effects clearly demonstrates the potential for dramatic scaling down and commercialization of atomic vapor cell-based technology, including for educational purposes.

This article is organized as follows. Section 2 gives a brief summary of the basic principles of idealized three-level EIT systems and typical experimental results for slow and stored light using warm atoms. Section 3 describes general algorithms for optimization of an EIT-based quantum memory based on slow and stored light and their recent experimental verification. Section 4 discusses modifications to the idealized description of EIT and slow/stored light arising from the motion of warm atoms, as well as related experiments involving buffer gas and wall-coated vapor cells. Experimental demonstrations of the storage of non-classical states of light in warm atomic ensembles are described in Sect. 5, in which there is also a discussion of additional complications that arise for non-classical signal storage compared to that of weak coherent signals. Section 6 provides a comparison of ensemble EIT schemes with alternative light storage techniques.

2. Overview of EIT and slow/stored light in warm atoms

2.1. Basic principles of EIT in an idealized three-level scheme

Following the formalism of [10], we consider propagation of a weak optical signal (or probe) pulse with envelope $\mathscr{E}(z,t)$ and a strong (classical) optical control field with a Rabi frequency envelope $\Omega(z,t)$ in a resonant Λ-type atomic medium, as illustrated schematically in Fig. 1. As in [6, 55, 57–59], we define the Rabi frequency Ω as

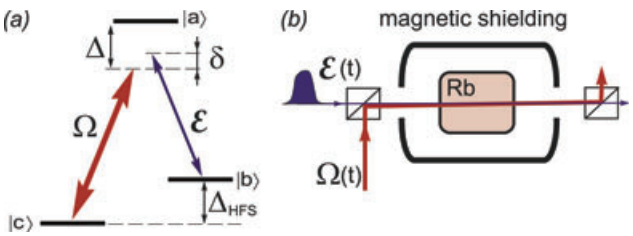

Figure 1 (online color at: www.lpr-journal.org) (a) Idealized three-level Λ EIT system, formed by interaction of an atomic ensemble with a strong control optical field $\Omega(t)$ and weak signal optical field $\mathscr{E}(t)$. Two-photon detuning δ is the mismatch between the frequency difference of the two optical fields and the energy splitting of the two ground-state levels $|b\rangle$ and $|c\rangle$ (usually a Zeeman and/or hyperfine splitting, $\Delta_{\rm HFS}$). One-photon detuning Δ is the common detuning of both optical fields from the excited state $|a\rangle$. (b) Typical arrangement for warm-atom EIT and slow/stored light experiments, with an atomic vapor cell (e. g., using Rb) located within magnetic shielding and interacting with the two optical fields.

$|\Omega|^2 = \wp_{\rm es}^2 I/(2\hbar^2\varepsilon_0 c)$, where I is the control intensity. In general, the propagation of a signal pulse can be described by the following equations [6, 10], assuming a slowly varying envelope $\mathscr{E}$ of the signal field and defining the optical polarization $P = \sum|b\rangle\langle a|/\sqrt{N}$ of the $|a\rangle$–$|b\rangle$ transition and the spin coherence $S = \sum|b\rangle\langle c|/\sqrt{N}$ between states $|b\rangle$ and $|c\rangle$:

$$(\partial_t + c\partial_z)\mathscr{E}(z,t) = ig\sqrt{N}P(z,t), \tag{1}$$

$$\partial_t P(z,t) = -\gamma P(z,t) + ig\sqrt{N}\mathscr{E}(z,t) + i\Omega(t - z/c)S(z,t), \tag{2}$$

$$\partial_t S(z,t) = -\gamma_{\rm bc} S(z,t) + i\Omega(t - z/c)P(z,t). \tag{3}$$

Here, c is the speed of light in vacuum, N is the number of atoms in the interaction region, γ and $\gamma_{\rm bc}$ are the decoherence rates of the optical and spin transitions, respectively, g is the atom-field coupling constant (assumed to be the same for both the $|a\rangle$–$|b\rangle$ and $|a\rangle$–$|c\rangle$ optical transitions), λ is the signal field wavelength, L is the length of the sample, and $\alpha L = 2g^2N/\gamma c$ is the unsaturated optical depth on the $|b\rangle$–$|a\rangle$ optical transition.

Under the conditions of two-photon Raman resonance (i. e., when $\nu_{\rm c} - \nu_{\rm s} = \Delta_{\rm bc}$) the control field creates strong coupling between the signal field $\mathscr{E}$ and a collective ground-state spin coherence ("spin wave") S in the atomic ensemble, which results in strong suppression of resonant absorption for both the control and signal fields; i. e., the effect known as EIT. In the ideal case of no spin decoherence ($\gamma_{\rm bc} = 0$) EIT provides 100% transmission of the optical fields. For any realistic system, however, nonzero $\gamma_{\rm bc}$ leads to residual absorption even under EIT conditions. In the case of steady-state optical fields and assuming no absorption for the strong control field Ω, the amplitude of the signal field after propagating the distance L along the axis z of the atomic medium $\mathscr{E}(z)$ is the following:

$$|\mathscr{E}(z)|^2 = |\mathscr{E}(0)|^2 \exp\left(-\alpha L \frac{\gamma\gamma_{\rm bc}}{2|\Omega|^2}\right). \tag{4}$$

For typical conditions in warm atoms, which provide a reasonable approximation of a three-level Λ system, EIT of more than 50% is readily accomplished. Note also that the full width at half maximum (FWHM) spectral bandwidth of the transparency window ($\Delta\omega_{\rm EIT}$) is proportional to the intensity of the control field [25, 26]:

$$\Delta\omega_{\rm EIT} = 2\frac{|\Omega|^2}{\gamma}\frac{1}{\sqrt{\alpha L}}. \tag{5}$$

The presence of the control field also modifies the dispersive properties of the atomic medium near the two-photon Raman resonance. In particular, EIT is accompanied by a steep positive variation $dn(\nu_{\rm s})/d\nu_{\rm s}$ of the refractive index n with the frequency $\nu_{\rm s}$ of the signal field. This sharp non-anomalous dispersion results in an ultraslow group velocity for the signal pulse. If the bandwidth of the signal pulse lies within the EIT spectral window, then the pulse will be delayed, with only modest absorption while propagating through the atomic medium of length L, by the group

delay t_D:

$$t_D = L/v_g = \alpha L \frac{\gamma}{2|\Omega|^2}. \quad (6)$$

Importantly, the intensity of the control field dictates the propagation (group) velocity of the signal pulse by determining the spectral width of the transparency window: the weaker the control field, the longer the group delay. Therefore, by adiabatically changing the intensity of the control field one is able to control the dynamics of the signal pulse with minimal loss. In particular, reducing the control field intensity to zero reduces the signal pulse group velocity to zero, effectively storing the information carried by the pulse in the atomic medium. It is convenient to describe such slow light propagation in terms of quasi-particles – "dark-state polaritons" [6, 10] – which treats the propagation of the signal pulse through the EIT medium via a quantum mechanical field operator $\Psi(z,t)$ that is a combination of photonic ($\mathscr{E}(z,t)$) and ensemble spin coherence ($S(z,t)$) components:

$$\Psi(z,t) = \cos(\theta)\mathscr{E}(z,t) - \sin(\theta)S(z,t), \quad (7)$$

where the mixing angle θ is defined as

$$\cos(\theta) = \frac{\Omega}{\sqrt{\Omega^2 + g^2 N}} = \sqrt{\frac{v_g}{c}}. \quad (8)$$

This treatment provides a simple description of stored light as a dark-state polariton tuned to be completely an ensemble spin coherence ($\cos(\theta) = 0$), which can be realized by reducing the control field to zero ($\Omega = 0$) once the signal pulse has entered the EIT medium. Such a pulse can be stored for times of the order of the ensemble spin coherence lifetime ($T_2 = 1/\gamma_{bc}$) and then converted back to a propagating slow light pulse by switching the control field back on ($\Omega \neq 0$, $\cos(\theta) \neq 0$) and released from the EIT medium as a purely photonic pulse. Quantum states of retrieved signal pulses are in principle identical to those of the input pulses.

Figure 2 illustrates schematically the three stages of the light storage process (writing, storage, and retrieval). At the writing stage, a signal pulse $\mathscr{E}_{in}(t)$ is mapped onto a collective spin excitation $S(z)$ by adiabatically reducing the control field to zero. This spin wave is then preserved for some storage time τ (storage stage); all optical fields are turned off at that time. Finally, at the retrieval stage, the signal field $\mathscr{E}_{out}(t)$ is retrieved by turning the control field back on.

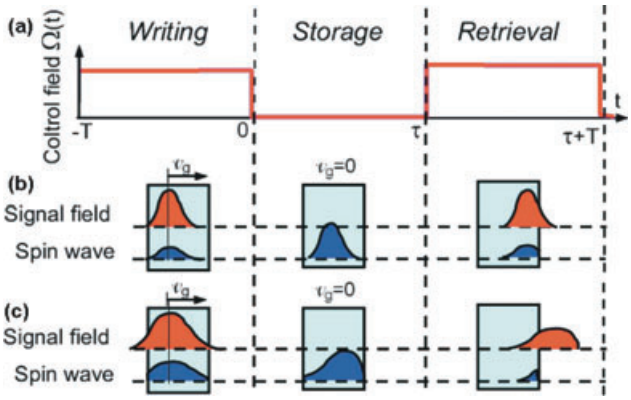

Figure 2 (online color at: www.lpr-journal.org) Schematic of the light storage process. (a) Time variation of the control field $\Omega(t)$, which is on during the writing and retrieval stages and is turned off for the storage period. (b) Light storage under ideal conditions (atomic medium with very high optical depth and insignificant loss), in which the signal field pulse is slowed down and fully compressed inside the EIT medium during the writing stage, and then completely mapped (stored) into the spin wave and finally retrieved without losses. (c) The same process for more realistic conditions (moderate optical depth, some loss); in this case the slow light group velocity v_g is not sufficiently small to compress the whole signal pulse inside the EIT medium, so that the front of the pulse escapes the cell before the control field is turned off; at the same time the tail of the pulse is not stored since it does not enter the medium during the writing stage. Practical considerations of the EIT medium length and possible pulse compression (proportional to the optical depth) set the fundamental limitation of maximum achievable light storage efficiency, even for insignificant loss during the storage period.

2.2. Experimental realization of EIT and classical slow/stored light in warm atomic ensembles

The idealized three-level Λ scheme can be closely realized in optical transitions of the D lines of alkali metal atoms, such as Rb and Cs. Either two hyperfine components of the ground state or Zeeman substates of the same hyperfine component can play the role of the two ground states $|b\rangle$ and $|c\rangle$ for a Λ system, such as shown in Fig. 1a. A typical arrangement for warm-atom EIT and slow/stored light experiments is shown in Fig. 1b. Since a stable relative phase between the control and signal fields is required to create, preserve, and retrieve long-lived spin coherence via EIT, these two fields are typically derived from the same laser to address a Zeeman coherence within the same hyperfine state, or from two phase-locked lasers tuned to the different hyperfine optical transitions. In typical experimental configurations, orthogonal control and signal fields are used; they are combined at a polarizing beam splitter before entering the vapor cell, and then the control field is separated after the cell using a second polarizer, so so that the signal field is separately detected.

For some experiments, it is possible to phase-modulate the output of a single laser at a microwave frequency matching the atomic hyperfine splitting, and then use the strong field at unmodulated frequency ν_c as the control field and one of the first modulation sidebands at frequency $\nu_c + \Delta_{HFS}$ as the signal field. In this case both fields perfectly spatially overlap and have the same polarization, but it is more challenging to isolate the signal field for detection after interaction with atoms. Often the signal and control fields are resolved by monitoring the beat frequency between each field and a third (reference) field at a shifted radio frequency. Another potential complication of this phase modulation

method is the presence of the other modulation sideband at the frequency $\nu_c - \Delta_{HFS}$. While this field is far-detuned from all optical transitions, its presence may still affect the signal field transmission and dynamics through enhanced four-wave mixing (FWM) processes (see discussion below).

Usually, an atomic vapor cell is a sealed Pyrex glass sphere or cylinder that contains a small amount of solid or liquid alkali metal. The density of atoms in the vapor phase is determined by thermodynamic equilibrium, and can be controlled by the cell temperature. In a "vacuum" cell, there is no buffer gas added and the alkali metal atoms move ballistically from wall to wall, except for occasional alkali metal-alkali metal collisions. Since atoms are usually completely thermalized as a result of a single collision with a wall, the atomic ground state coherence lifetime in a vacuum vapor cell is limited by the mean time-of-flight of atoms through the laser beam: $\gamma_{bc} \propto \langle v \rangle_T / a$, where a is the radius of the beam and $\langle v \rangle_T = \sqrt{8kT/\pi m}$ (where k is the Boltzmann constant, m is atomic mass, and T is absolute temperature) is the mean atomic velocity in thermal equilibrium. There are two commonly employed methods to extend the coherence lifetime of warm atoms: (i) atomic motion can be effectively slowed down by the use of an inert buffer gas, causing alkali metal atoms to move diffusively through the laser beam; or (ii) the atomic ground-state coherence can be preserved during wall collisions by coating the inside of the glass walls with an anti-relaxation coating. With the buffer gas method the atom-laser interaction time can be extended by several orders of magnitude [27, 28]:

$$\gamma_{bc} = 2.405^2 \frac{D}{a^2} \frac{1}{1 + 6.8\lambda/a}, \qquad (9)$$

where $D = D_0 \cdot p_0/p$ is the diffusion constant for motion of the alkali metal atom through the buffer gas, $\lambda = 3D/\langle v \rangle_T$ is the alkali metal atom mean free path, p is the buffer gas pressure, and D_0 and p_0 are the corresponding values at one standard atmosphere. Standard buffer gases include inert atoms (He, Ne, Ar) or simple molecules (N_2); these gases are characterized by small collisional dephasing cross-section for the ground states of alkali metal atoms (detailed information on diffusion constants and collisional cross-sections of alkali metal atoms with various buffer gases is available, for example, in [27]). However, excited electronic states are much more sensitive to buffer gas collisions, resulting in a homogeneous broadening of the optical transitions.

Figure 3 shows typical experimental results for slow and stored light in a ^{87}Rb vapor cell, with 22 torr of Ne buffer gas in this example. A single laser tuned in the vicinity of the $5S_{1/2} \rightarrow 5P_{1/2}$ (D1) line of ^{87}Rb served as the control optical field. Phase modulation of the laser output using an electro-optical modulator transferred approximately 2% of the total light power into each first-order sideband, creating signal and Stokes optical fields with negligible variations in control field amplitude. Small variation of the modulation frequency around the hyperfine splitting of 6.835 GHz controlled the two-photon detuning δ; and desired pulse shapes for the signal field were produced by applying a calibrated voltage to the modulator during the writing stage. In such a

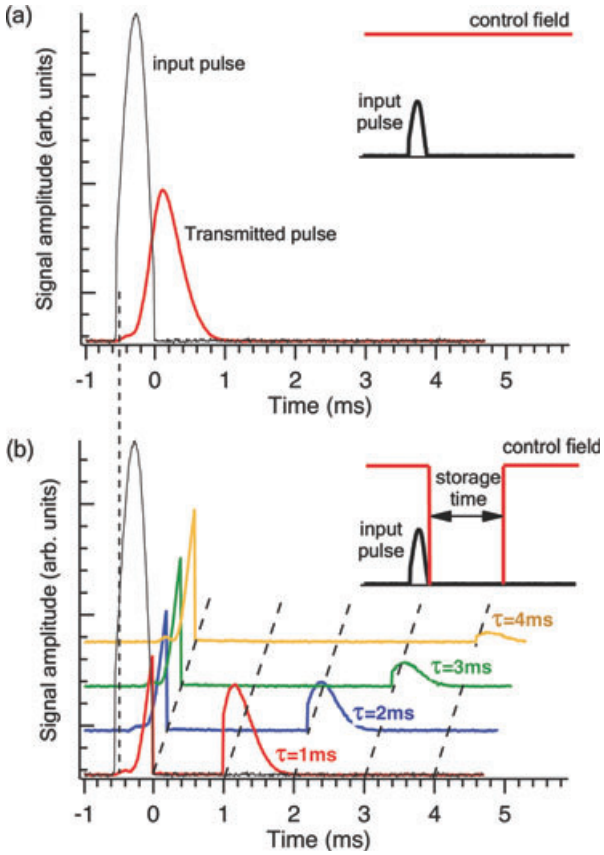

Figure 3 (online color at: www.lpr-journal.org) Examples of measured signal field after propagation through a warm-Rb EIT medium with with 22 torr Ne buffer gas: (a) slow light (constant control field); (b) stored light (flat control field during signal pulse writing and retrieval; zero control field during storage). In both cases the control field power was 900 μW. Insets show schematics of time-course for the control field and input signal pulse.

configuration the best slow and stored light was observed using circularly polarized optical fields in a Λ system formed by the control field on the $F = 2 \rightarrow F' = 2$ transition and the signal field on the $F = 1 \rightarrow F' = 2$ transition.

In slow light experiments the control field intensity is ideally constant; hence the signal pulse propagates with constant reduced group velocity. Figure 3a shows a measured delay of 440 μs for the output signal pulse, exceeding the FWHM of the input pulse (350 μs), with a corresponding fractional delay of 1.3. However, interaction with the atomic ensemble also broadened the output signal pulse to 500 μs due to the finite EIT transmission linewidth. In the most common stored light realization (Fig. 3b) the control field is constant during writing and retrieval stages ("flat" control); but it is turned off during the storage using, for example, an acousto-optical modulator. In such cases the signal pulse, slowly propagating inside the atomic ensemble as a dark-state polariton, is converted into a non-propagating spin wave (i. e., is "stored" in the atomic medium) by turning off the control field power. In the experimental example shown in Fig. 3b, the front portion of the signal pulse escaped the cell before storage due to insufficient fractional

delay and pulse broadening ("leakage"). The stored fraction of the signal pulse was then retrieved by turning the control field back on after a few milliseconds. The shapes of the retrieved signal pulses were nearly identical; they also were good matches to the slow light pulse shown in Fig. 3a (accounting for the missing front of the signal pulse due to leakage). However, longer storage time resulted in exponential reduction of the recovered signal pulse energy due to spin wave decoherence during storage. Relatively long (> 1 ms) measured spin coherence lifetimes have been achieved in warm-atom EIT-based stored light experiments by using high-quality magnetic shielding to minimize the effect of stray laboratory magnetic fields, and by mitigating the effect of atomic thermal motion using a relatively large laser beam diameter (approximately 1 cm) and high buffer gas pressure [17, 29].

Substantially longer spin coherence lifetimes are achievable in vapor cells with an anti-relaxation wall coating. Paraffin is the most commonly used anti-relaxation wall coating for alkali metal atom vapor cells [30–33]. Ground-state coherence times of up to a second (i. e., up to 10 000 wall collisions before spin decoherence) were achieved using paraffin-coated cells [30, 32, 34–36], and a Zeeman coherence lifetime of up to 60 s was recently reported in vapor cells with novel alkene coatings [37]. However, the dynamics of light-atom interactions is more complicated with wall-coated cells than with buffer gas cells due to long coherence lifetimes "in the dark" (outside the laser beam), as is discussed in more detail in Sect. 4.

At low optical depth (i. e., low atomic density and/or small vapor cell length) the ground-state coherence lifetime is mainly determined by environmental parameters such as the finite interaction time of atoms with the optical fields, residual magnetic field inhomogeneities, atom-atom and atom-wall collisions [27], etc. At high optical depth, however, other processes can become dominant and shorten the ground-state coherence lifetime, e. g., radiation trapping [38–40]. Due to residual absorption at finite optical depth there is a nonzero population of the excited atomic state in the presence of the optical fields, even under EIT conditions, resulting in spontaneous emission of photons in arbitrary directions and with arbitrary phases. These spontaneously emitted photons do not generally experience EIT due to wave-vector mismatch with the control field. Thus in optically thick vapor there is a high probability for such photons to be reabsorbed, leading to further spontaneous emission, reabsorption, etc. Such "radiation trapping" can significantly degrade the dark state that underlies EIT.

At high atomic density, EIT performance can also be degraded by competing nonlinear processes, such as stimulated Raman scattering and four-wave mixing (FWM) [25, 41–46]. In this case one cannot neglect the off-resonant coupling between levels $|b\rangle$ and $|a\rangle$, which results in generation of a Stokes optical field at the frequency $\nu_c - \Delta_{HFS}$. Such a situation is well modeled by a simple double-Λ system, where the output signal and Stokes field amplitudes are the results of interference between "traditional" EIT and FWM [25, 41, 47, 48]. Both continuous-wave EIT spectra and signal pulse propagation dynamics can be affected by the presence of a seeded or spontaneously generated Stokes field, with both signal and Stokes fields observed at the reading stage of the light storage process [49–51]. On the other hand, such FWM processes can be used to create strong correlation and entanglement between the signal and Stokes fields [52–54].

3. Optimization of light storage efficiency

3.1. Limited memory efficiency due to finite optical depth

We define the light storage memory efficiency η as the probability of retrieving an incoming single photon after storage in an ensemble EIT system; or, equivalently, as the energy ratio between the initial and retrieved signal pulses [55, 56]:

$$\eta = \frac{\int_{\tau}^{\tau+T} |\mathscr{E}_{\rm out}(t)|^2 {\rm d}t}{\int_{-T}^{0} |\mathscr{E}_{\rm in}(t)|^2 {\rm d}t}. \qquad (10)$$

Even under the idealized assumptions of no incoherent losses in the system, realization of an EIT quantum memory with 100% storage efficiency requires simultaneous fulfillment of two conditions. First, as illustrated in Fig. 2b, the group velocity v_g of the signal pulse inside the medium has to be low enough to spatially compress the entire input pulse within the length L of the ensemble, i. e., to avoid "leaking" the front edge of the signal pulse past the EIT medium or cutting off the pulse tail when the control field is shut off as part of the storage procedure. This first condition equates to requiring the signal pulse duration T to be short enough so that $Tv_g \ll L$. The second condition is that all spectral components of the incoming signal pulse must fit inside the EIT window to minimize absorption and resulting spontaneous emission losses, which equates to requiring $1/T \ll \Delta\omega_{\rm EIT} \simeq \sqrt{\alpha L} v_g/L$ [6]. The simultaneous satisfaction of both conditions is possible only at very high optical depth $\alpha L \gg 1$ [6, 55]. As mentioned above, it is very challenging to maintain high transparency and long ground-state coherence time as the density of atoms increases. Thus, for practical purposes it is important to optimize EIT memory performance for moderately high optical depth $\alpha L > 1$. Such an imperfect but "realistically optimized" situation is illustrated in Fig. 2c: the tails of the signal pulse are not stored in the EIT medium due to finite optical depth; there is some modest decoherence during storage; and the output pulse shape is slightly modified due to finite EIT spectral width. Degradation due to these factors must be balanced to achieve maximum signal pulse storage efficiency.

3.2. Optimization procedure

In a series of recent theoretical works, Gorshkov et al. considered a wide range of processes for optimal storage and retrieval of photon wave packets in atomic ensembles [55, 57–60]: EIT; far-off-resonant Raman; and a variety of spin echo methods including ensembles enclosed in

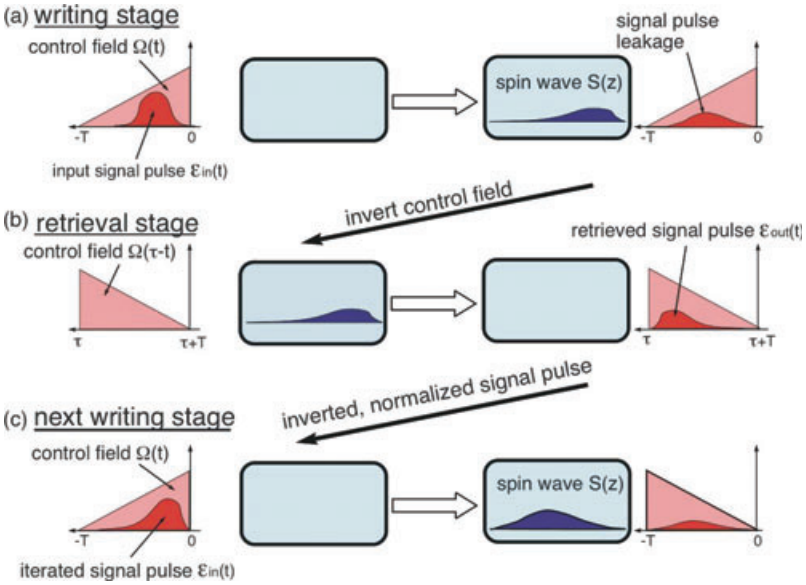

Figure 4 (online color at: www.lpr-journal.org) Schematic of the iterative signal pulse optimization procedure. (a) An input signal pulse $\mathscr{E}_{\text{in}}(t)$ is mapped into a spin wave $S(z)$ using a control field envelope $\Omega(t)$. (b) After a storage period τ, the spin wave is mapped into an output signal pulse $\mathscr{E}_{\text{out}}$ using the time-reversed control field envelope $\Omega(\tau - t)$. (c) The time-reversed and normalized version of the measured $\mathscr{E}_{\text{out}}$ is used as the input $\mathscr{E}_{\text{in}}$ for the next iteration of the procedure. (Reproduced from [56].)

a cavity, inhomogeneous broadening, and high-bandwidth non-adiabatic storage ($1/T \sim \alpha L\gamma$) [60]. This comprehensive analysis revealed several general strategies for stored light optimization; and demonstrated that the highest achievable memory efficiency depends fundamentally only on the optical depth αL, since the strength of the photonic coupling to the collective excitation in the atomic ensemble, relative to spontaneous decay, increases with optical depth [55]. The analysis of Gorshkov et al. also showed that under optimized conditions the writing stage is the time reversal of the retrieval stage. This time reversal symmetry implies that for degenerate lower levels of a Λ system, stored signal pulses are optimally retrieved by a control field propagating in the opposite direction with respect to the writing stage (i. e., "backward retrieval") [55,58]. In contrast, "forward retrieval" (co-propagating writing and retrieval control fields) is more efficient when non-degenerate hyperfine states are used for light storage [58], due to the nonzero momentum of the spin wave for a non-degenerate Λ system.

Furthermore, the analysis mentioned above demonstrated that for each optical depth, there exists a unique spin wave $S_{\text{opt}}(z)$ that provides the maximum memory efficiency. Thus, the focus of the optimization process becomes the identification of a matched pair of control and signal pulse fields to map the signal pulse reversibly onto the optimal spin wave.

Two solutions have been analyzed [55, 58] for this optimization problem. The first method utilizes the time-reversal symmetry of the optimized storage process, which enables determination of an optimal signal pulse shape for a given control field temporal profile using successive time-reversal iteration of the signal pulse shape. An important advantage of this optimization method is that its realization does not require any prior knowledge of the system parameters. Figure 4 shows schematically the iterative optimization procedure adapted to forward retrieval [58]: the input signal pulse $\mathscr{E}_{\text{in}}(t)$ is mapped into a spin wave $S(z)$ inside the atomic vapor for a given optical depth and control Rabi frequency envelope $\Omega(t)$ (both $\mathscr{E}_{\text{in}}(t)$ and $\Omega(t)$ are assumed to vanish outside of time interval $[0, T]$); an output signal pulse $\mathscr{E}_{\text{out}}(t)$ is forward-retrieved using the time-reversed control field pulse $\Omega(T - t)$; then a time-reversed and normalized version of the retrieved signal pulse $\mathscr{E}_{\text{out}}(T - t)$ becomes the input signal pulse for the next iteration cycle.

These steps are repeated several times until the shape of the retrieved pulse $\mathscr{E}_{\text{out}}(t)$ is identical to the time-reversed input signal pulse $\mathscr{E}_{\text{in}}(T - t)$ (attenuated because of imperfect memory). Under reasonable assumptions (we assume that writing and retrieval control fields are real, and that spin decoherence has a negligible effect during storage and retrieval stages, and only cause a modest reduction of the efficiency due to spin wave decay during storage time) the resulting pulse shape provides the highest storage efficiency possible for a given optical depth and control field profile. The success of this optimization procedure is based on linearity of the EIT light storage process, such that at each step the stored spin wave can be decomposed into a linear superposition of orthogonal spin wave eigenmodes, for which the optimal spin wave results in maximum storage efficiency, and consequently maximum contribution to the retrieved signal pulse. Thus, after several iterations the optimization procedure converges to the optimized input signal pulse shape for a given optical depth and control field temporal profile.

The second optimization method allows maximally efficient storage and retrieval of an arbitrary signal pulse shape $\mathscr{E}_{\text{in}}(t)$, which requires determination of an optimized control field $\Omega(t)$. As shown in [58], this optimized control field can be most easily calculated for the idealized condition of mapping $\mathscr{E}_{\text{in}}(t)$ into a "decayless" spin wave $S(z)$ in a semi-infinite atomic EIT medium with no optical polarization decay and for a given optical depth αL. This decayless spin wave $S(z)$ allows unitary reversible storage of an arbitrary input signal pulse, which establishes a one-to-one correspondence between $\mathscr{E}_{\text{in}}(t)$ and a given control field. As also shown in [58], this same control field maps the input signal pulse onto the optimal spin wave $S_{\text{opt}}(z)$ in a realistic EIT medium with finite length and polarization decay.

3.3. Experimental verification

The light storage optimization procedures outlined above have been successfully tested experimentally using weak classical signal pulses in warm Rb atomic ensembles. Experimental realizations [49,56] of the iterative time-reversal optimization method confirmed the three primary predictions of the underlying theory [55, 58]: (i) efficiency increases with each iteration until the input signal field converges to its optimal pulse shape; (ii) the result of the optimization procedure is independent of the initial (trial) signal pulse shape; and (iii) the final, optimal light storage efficiency depends only on the optical depth and not on the control field temporal profile.

An example experimental realization of the iterative optimization procedure is shown in Fig. 5. The initial input signal pulse had a Gaussian profile (iteration 0). Since this pulse shape was far from optimal, a large fraction of the input signal pulse escaped the cell before the control field was turned off. However, some of the pulse was stored as an atomic spin wave (iteration 0, writing stage). After a 400 µs storage interval, the time-reversed control field was turned on (iteration 0, retrieval stage), and the retrieved signal pulse was detected. The efficiency of the storage process at this stage was only 16%. The detected signal pulse shape in iteration 0 was then digitally reversed and normalized to the same integrated input pulse energy and used as an input signal pulse for iteration 1. This new input pulse shape was much closer to optimal, such that it was stored with an efficiency of 45%. To find the optimal input pulse shape, these steps were repeated several times until the shape of the retrieved signal pulse was identical to the reversed profile of the input pulse (though the amplitude of the retrieved pulse was always somewhat attenuated because of finite loss in the EIT medium unrelated to pulse shape). The resulting signal pulse shape provided the highest storage efficiency for a given control field (and fixed optical depth). For example, in the experiment shown in Fig. 5, the optimal signal field pulse shape (achieved at the end of iteration 2) yielded a storage efficiency of 47%.

In this and all other experiments the resultant optimized signal pulse shapes are in excellent agreement with theoretical calculations using Eqs. (1)–(3) and effective parameters for the optical depth and control field Rabi frequency [49] to make a connection between realistic ^{87}Rb atoms (which have 16 unique states associated with the D1 optical transition) and an idealized three-level Λ system. Similarly, optimized control field envelopes obtained from numerical solutions of Eqs. (1)–(3) for arbitrary signal pulses provide light storage efficiency similar to that of the iterative signal pulse method. Figure 6 shows examples of measured light storage for two randomly chosen signal field envelopes using the calculated optimal control fields for the writing stage and two different retrieval methods. First, a flat retrieval control field of the same intensity was used to retrieve both pulses, which resulted in the same output pulse (red dashed

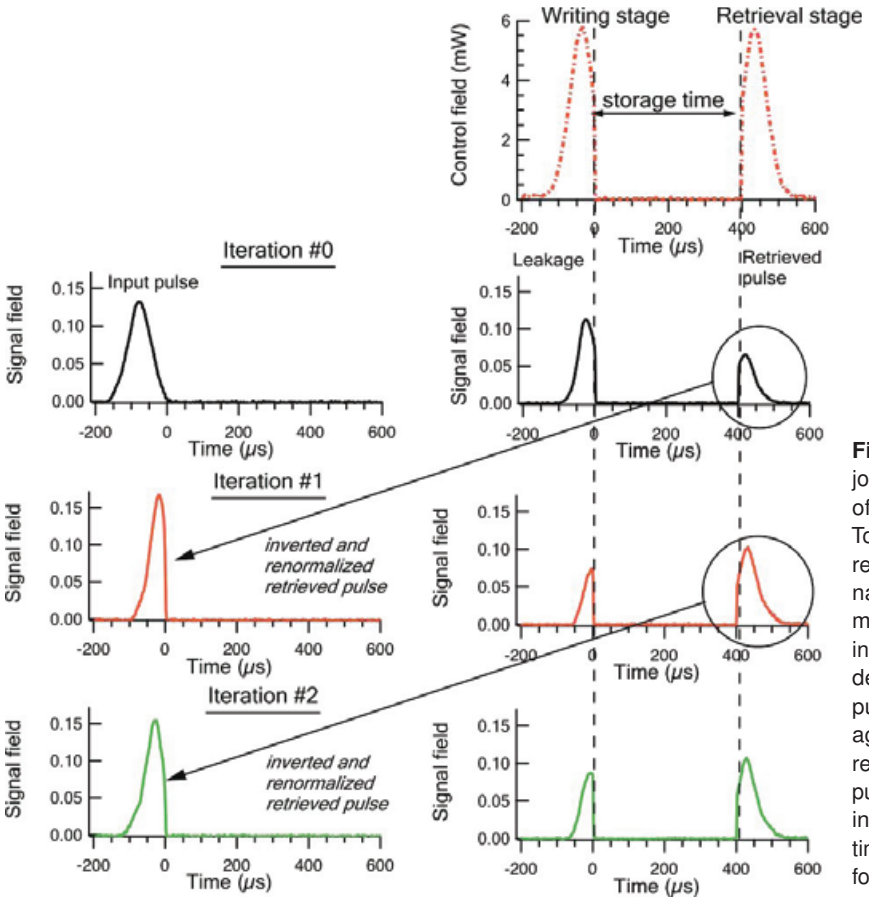

Figure 5 (online color at: www.lpr-journal.org) Example experimental realization of the light storage optimization procedure. Top row: control fields during the storage and retrieval process. Lower three rows: input signal pulses during three iterations of the optimization process in the left column with the initial input pulse in the first row and the pulses derived from the previous iteration's output pulse in the following rows. Signal field leakage during the write process as well as the retrieved pulse are shown on the right. Signal pulses are normalized such that the integrated intensity of the input signal pulse is unity for time measured in microseconds. For more information, see [61].

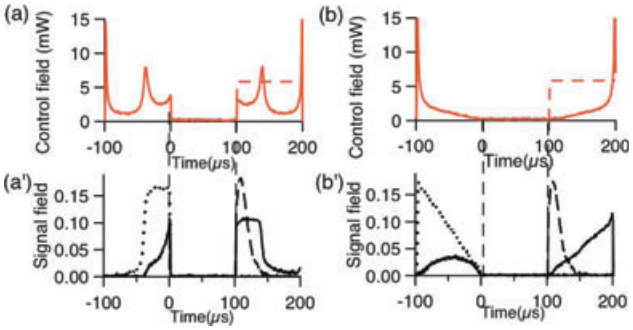

Figure 6 (online color at: www.lpr-journal.org) Example measurements of light storage for two differently shaped signal pulses (a′, b′) using in each case the calculated optimal control fields (a, b) for the writing stage ($t < 0$). Input signal pulse shapes are shown as black dotted curves. The same graphs also show the signal pulse leakage (solid black curves for $t < 0$) and retrieved signal pulses using flat control fields (red dashed curves) or time-reversed control fields (red solid curves) at the retrieval stage ($t > 100\,\mu s$). The temperature of the Rb vapor cell was 60.5 °C ($\alpha L = 24$); other experimental details are given in [49].

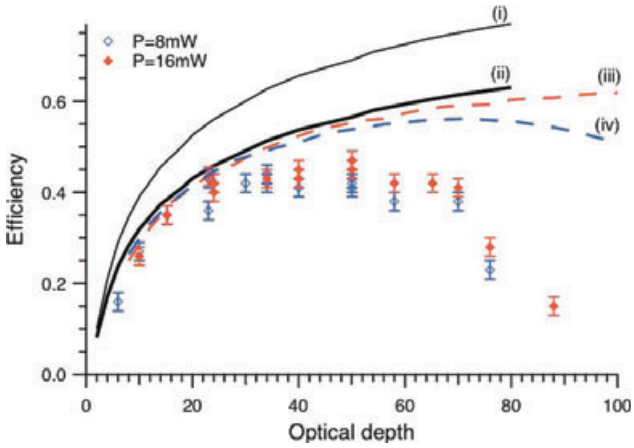

Figure 7 (online color at: www.lpr-journal.org) Measured light storage efficiency as a function of optical depth (colored diamonds) for two different power values of flat control fields, optimized signal pulses, and a 100 μs storage period in warm Rb vapor [49]. Thin and thick lack solid curves show the theoretically predicted maximum efficiency for both high and low control field powers, assuming no spin wave decay (i) and taking into account an efficiency reduction by a factor of 0.82 during the 100 μs storage period (ii). Dashed red (iii) and blue (iv) curves are calculated efficiencies for the same two control fields assuming spin wave decay with a 500 μs time constant during all three stages of the storage process (writing, storage, retrieval) [49].

curves in Figs. 6a′ and b′) independent of the input signal pulse shape, because the excitation was stored in the same optimal spin wave in each case. Second, an optimal control field was used for retrieval (i. e., a time-reversed version of the writing control field), which yielded output signal pulses that were time-reversed copies of the corresponding input signal pulses (moderately attenuated due to finite loss in the system). This observed time-reversal symmetry between stored and retrieved signal pulse shapes illustrates the mutual consistency of the two optimization methods.

Experimental tests have also been performed of the theoretical prediction of light storage memory efficiency increasing with optical depth, by repeating the iterative signal pulse optimization procedure for a wide range of warm Rb atomic densities [49]. Figure 7 shows memory efficiency as a function of optical depth measured for two different power values of a flat control field. Each experimental data point corresponds to the storage efficiency measured for optimized signal pulses obtained using the iterative optimization procedure for each particular control field power and optical depth. These results indicate that for moderately low optical depth ($\alpha L \leq 25$) the optimization procedure follows the prediction of the simple theory, yielding a maximum efficiency that is independent of control field power, reaching a highest efficiency of 45%. However, at higher optical depth the experimental results deviate from theory, showing reduced light storage efficiency at high optical depth. Several reasons for this non-ideal behavior have been identified. One of them is decay of the spin wave. Nonetheless, if the signal pulse duration is short enough, the effect of spin wave decay is negligible during the writing and retrieval processes; and the optimization procedures, developed for an ideal system with no spin decay, can apply to realistic atomic ensembles with spin decoherence. In all cases, maximum storage efficiency is achieved for optimal signal and/or control field pulse shapes after taking into account the reduction of storage efficiencies by the factor $e^{-\tau/t_s}$ due to spin wave decoherence during the storage time τ (t_s is the spin wave decay time constant). Note that as the optimal pulse duration increases with optical depth for a given control power, due to density narrowing of the EIT window (see Eq. (5)), spin decay also becomes significant during writing and retrieval, breaking time-reversal symmetry and reducing the efficiency of light storage at higher optical depth. This problem can be alleviated in many practical cases by using higher control field power, and hence shorter optimal signal pulses.

Fig. 7 also shows that spin wave decay cannot account for the observed lower-than-expected optimized storage efficiency for $\alpha L \geq 25$, although time-reversal symmetry is still preserved [49]. One of the possible causes for the lower efficiency is resonant FWM, which becomes significant at large optical depth. This process is well modeled by a simple double-Λ system, where the output signal and Stokes field amplitudes are the results of interference between the "traditional" (single-Λ) EIT system and their coupled propagation under FWM conditions. The description of the coupled propagation of the signal and Stokes fields is in good agreement with experimental observations [48, 51]. Under these conditions the simple dark-state polariton treatment of light storage is no longer valid. The spin wave becomes dependent on a combination of signal and Stokes fields, which does not preserve each of them individually [50, 51]. While detrimental for storage of quantum states of light, resonant FWM may be useful for classical slow light applications, as it offers additional control mechanisms for signal pulse propagation by, for example, controlling the amplitude of a seeded Stokes field. Moreover, by tuning

the central frequency of the input signal field around the two-photon resonance, one can achieve longer pulse delay and/or amplification [48]. Finally, note that for very high optical depth both optimization procedures fail when control field absorption becomes significant.

3.4. Pulse-shape control

The optimization methods outlined above can be employed together to help satisfy the two key requirements for a practical light storage quantum memory: (i) reaching the highest possible memory efficiency in an ensemble with finite optical depth and loss; and (ii) precisely controlling the temporal envelope of the retrieved signal pulse. The latter goal can be achieved by adjusting the control field envelopes for both writing and retrieval stages. Since the maximum memory efficiency is achieved when the input signal pulse is mapped onto an optimal spin wave $S(z)$, determined by an optimal control field $\Omega(t)$ that is unique for each αL [55, 58], the *retrieval* control field $\Omega(t)$ $(\tau < t < \tau + T)$ that maps $S(z)$ onto the desired target output signal pulse $\mathscr{E}_{\rm tgt}(t)$ can be determined by the same control field optimization procedure together with the time-reversal symmetry principle for optimized light storage [49,55,56,58]. Thus the control field that retrieves the optimal spin wave $S(z)$ into $\mathscr{E}_{\rm tgt}(t)$ after storage is the time-reversed copy of the control field that stores the time-reversed target pulse $\mathscr{E}_{\rm tgt}(\tau - t)$ into $S(z)$ [62].

As shown in Fig. 8, this method has been employed experimentally for warm Rb atoms to achieve signal-pulse-shape-preserving storage and retrieval, i. e., a target output signal pulse that is identical to the input pulse when accounting for finite loss during the storage process [62]. The measured output signal pulse (solid black curve in Fig. 8b) matches very well the target "positive ramp" pulse shape (dashed blue line in Fig. 8b). Moreover, since this method is based on universal symmetries for optimal light storage, it is likely to be indispensable for applications in both classical [63] and quantum optical information processing in a wide range of experimental arrangements, such as ensembles enclosed in a cavity [57, 64], the off-resonant regime [55, 57, 58], non-adiabatic storage (i. e., storage of pulses of high bandwidth) [60], and ensembles with inhomogeneous broadening [59], including Doppler broadening and line broadening in solids.

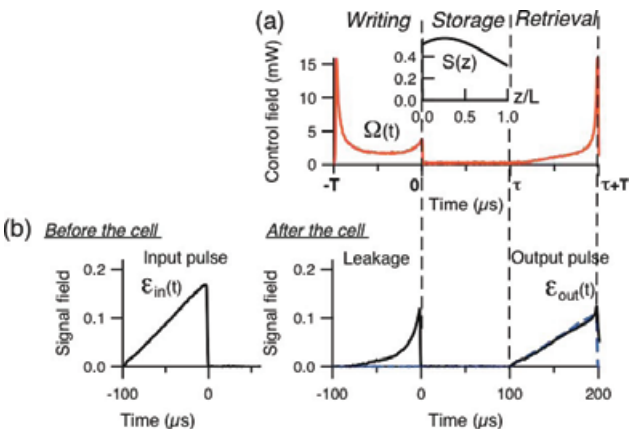

Figure 8 (online color at: www.lpr-journal.org) Measured (a) control and (b) signal fields in pulse-shape-preserving storage of a "positive ramp" signal pulse in warm Rb vapor using a calculated optimal control field envelope $\Omega(t)$. During the *writing* stage $(t < 0)$, the input pulse $\mathscr{E}_{\rm in}(t)$ is mapped onto the optimal spin wave $S(z)$ (inset in (a)), while a fraction of the pulse escapes the cell (leakage in (b)). After a *storage* time τ, the spin wave $S(z)$ is mapped into an output signal pulse $\mathscr{E}_{\rm out}(t)$ during the *retrieval* stage. The dashed blue line in (b) shows the target output pulse shape calculated for realistic conditions in this experiment; see [62] for details.

4. Effects of EIT lineshapes on slow and stored light

4.1. Using measured EIT spectra to determine slow-light delay

Characterization of slow and stored light for a particular medium often begins with the associated static EIT resonance. Recent work [65] has shown that a simple realistic model of EIT spectra allows accurate prediction of the slow-light pulse delay from two easily measurable parameters: the linewidth and the off-resonant transmission level (which serves as a proxy for the medium's effective optical depth). Fig. 9a shows a typical measured EIT spectrum for warm Rb atoms, with the signal field transmission normalized to the two-photon off-resonance transmission. For a Lorentzian EIT lineshape, the optical depth of the medium αL can be determined from the two-photon off-resonance transmission "floor" F of the EIT spectrum: $F = \exp(-\alpha L)$. Also, the EIT FWHM linewidth W and peak transmission $1 - C$ together determine the coherence decay and optical pumping rate. The predicted maximum slow-light delay τ can then be expressed from the above easily measurable parameters as $\tau_{\rm max} = -\ln(F)/W$. As shown in Fig. 9b, good agreement is found between the measured maximum slow-light delay and the delay predicted from the simple model of [65] using easily measured EIT spectrum parameters. In general, slow light with large pulse delay and high transmission efficiency is obtained for a low EIT spectral floor F (i. e., high optical depth) and large EIT transmission amplitude A (i. e., low loss). Thus the above characterization procedure using static EIT lineshape measurements can be an efficient, practical method to optimize slow light performance. This technique should be applicable to a wide range of slow light media, for which static resonance lineshapes can be easily extracted.

Note that the above procedure is quantitatively valid for a Lorentzian (or near-Lorentzian) EIT lineshape, but can be still used as a qualitative guide for non-Lorentzian lineshapes. In practice, several factors can cause a non-Lorentzian EIT lineshape, such as atomic motion, a non-uniform laser beam profile [66, 67], FWM effects [25, 47, 48, 68], and various other spectral narrowing and reshaping phenomena [26].

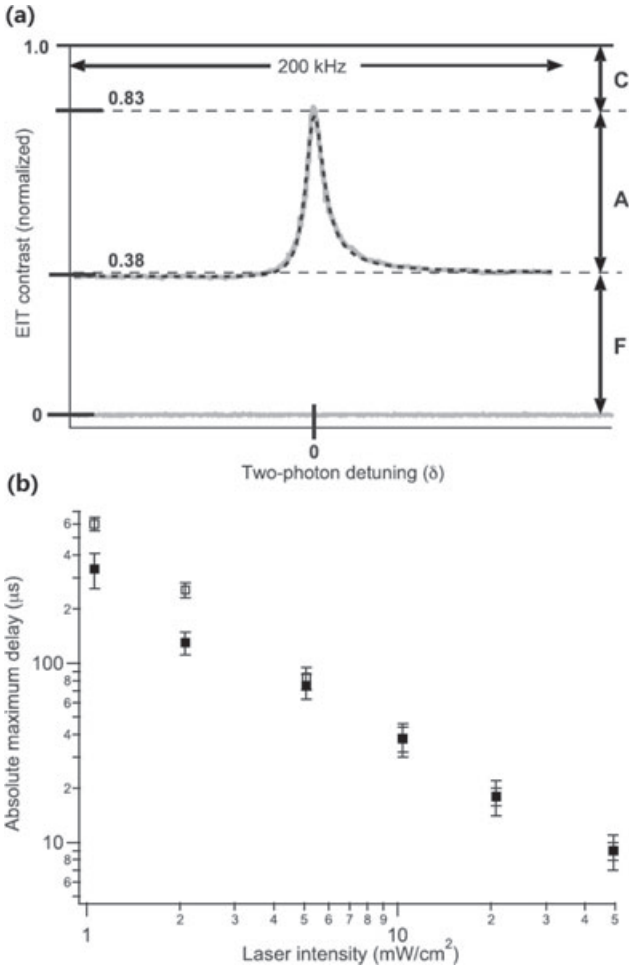

Figure 9 (a) Example measured EIT intensity spectrum for warm Rb vapor with normalized contrast and background levels. The solid gray curve represents the data while the black dashed curve is a fit to a skew-Lorentzian yielding an EIT FWHM linewidth $W \simeq 10\,\text{kHz}$. F: signal intensity above background away from EIT resonance (the "floor"); A: amplitude of EIT peak; C: difference between EIT peak and 100% transmission (the "ceiling"). (b) Measured slow-light delays (filled squares) and predictions (open squares) based on experimentally accessible EIT lineshape parameters. Good agreement is shown over a large range of pulse delays and laser intensities. (Reproduced from [65], which also includes experimental and model details.)

We next focus on the effects of atomic motion in buffer and coated cells on EIT spectra, slow light dynamics, and stored light efficiency.

4.2. Ramsey-narrowed EIT lineshapes in buffer gas cells

To increase the atom-light interaction time in warm vapor cells, an inert buffer gas at a pressure of a few torr is often added to restrict the fast, thermal atomic motion. A buffer gas also reduces two-photon Doppler broadening of the EIT medium's optical transitions through the Dicke narrowing

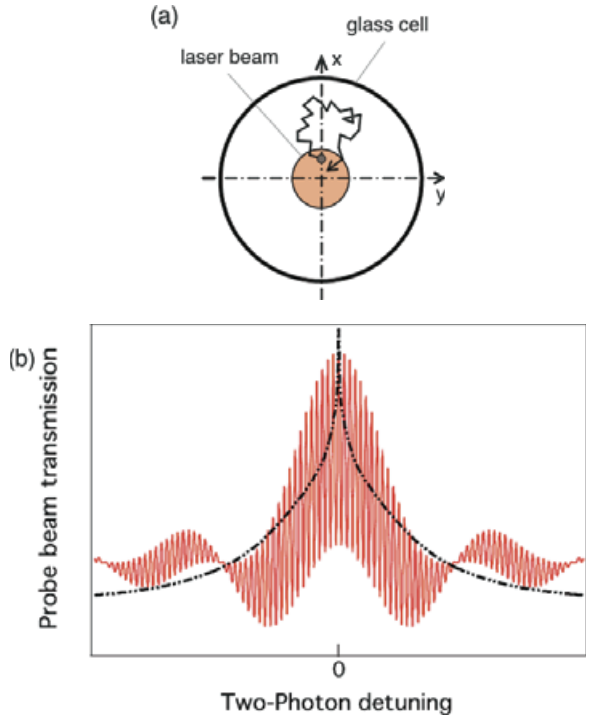

Figure 10 (online color at: www.lpr-journal.org) (a) Example path for atoms diffusing in and out of the laser beam in a buffer gas cell. (b) Calculated EIT lineshapes resulting from diffusive return of atomic coherence to the laser beam. The solid red curve is an example for one particular diffusion history (Ramsey sequence), with equal time spent in the laser beam $t_{\text{in}} = \tau_{\text{D}}$ before and after diffusing in the dark for time $t_{\text{out}} = 20\tau_{\text{D}}$, where τ_{D} is the mean time to leave the beam given by the lowest-order diffusion mode. The dashed black curve is the weighted average over all Ramsey sequences, yielding the characteristic "pointy" EIT lineshape resulting from diffusion-induced Ramsey narrowing. (Reproduced from [70].)

effect [69]. It has been common practice to calculate EIT decoherence due to atom diffusion out of the laser beam using only the lowest diffusion mode, as in Eq. (9), which yields a Lorentzian EIT lineshape in the non-power-broadened regime. Note, however, that this lowest diffusion mode calculation implicitly assumes that there is insignificant diffusive return of atomic coherence to the laser beam – an assumption that is often incorrect for practical warm-atom EIT systems. In particular, when the laser beam diameter is much smaller than that of the vapor cell and other decoherence processes (e. g., due to inhomogeneous magnetic fields) are insignificant, atoms can diffuse in and out of the laser beam multiple times without losing their coherence, as shown schematically in Fig. 10a. In this case, each atom in the EIT ensemble effectively experiences a Ramsey-like sequence of interactions with the laser interspersed with coherent evolution in the dark (outside the laser beam). The resultant contribution of one such sequence to the EIT spectrum is well modeled by Ramsey fringes, as shown in Fig. 10b. Summing over contributions to the EIT spectrum from all atoms undergoing such diffusive motion in and out of the laser beam, and using probabilistic weights

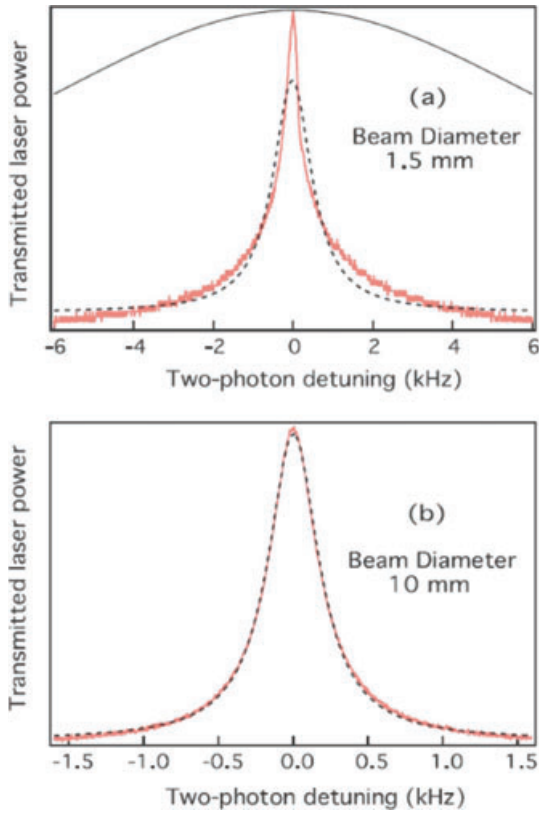

Figure 11 (online color at: www.lpr-journal.org) Measured Rb EIT lineshapes (red curves) and fits using a Lorentzian lineshape (dashed curves), with laser beam diameters of approximately (a) 1.5 mm and (b) 10 mm in a 3 torr Ne cell with total incident laser intensity of 1 μW/mm^2. Fitted Lorentzian parameters are the amplitude, off-resonant background, and full widths of approximately (a) 1400 Hz and (b) 400 Hz. The broad solid curve in (a) is a 20 kHz FWHM Lorentzian, the expected lineshape for a coherence lifetime set by the lowest order diffusion mode out of the laser beam, with amplitude set equal to the peak measured amplitude for illustrative purposes. (Reproduced from [70].)

for different Ramsey fringe spectra governed by the diffusion equation, one derives a non-Lorentzian, "pointy" EIT lineshape, with a sharp central peak that results from constructive interference of the central fringes of all diffusing atoms together with largely destructive interference of the other Ramsey fringes [70].

Both experiment and theory have demonstrated the existence and ubiquity of this "diffusion-induced Ramsey-narrowing" effect in warm-atom buffer gas EIT systems. As shown in Fig. 11a for typical Rb EIT operating conditions in a buffer gas cell, the measured EIT resonance for a 1.5 mm diameter laser beam has a FWHM of 740 Hz, whereas the calculated FWHM is approximately 20 kHz if one assumes (incorrectly) that the coherence lifetime is set by the lowest order diffusion mode out of the beam. As also shown in Fig. 11a, the measured EIT lineshape for the 1.5 mm diameter laser beam is spectrally narrower near resonance than a Lorentzian lineshape: this sharp central peak is the characteristic signature of diffusion-induced Ramsey narrowing. In contrast, the measured EIT resonance in the same buffer gas Rb cell for a 10 mm diameter laser beam (with the same total intensity as the 1.5 mm beam) is well fitted by a Lorentzian line shape with FWHM of 400 Hz (see Fig. 11b), which is in good agreement with the calculated FWHM using the lowest order diffusion mode, and is consistent with only a small fraction of atoms leaving this relatively large diameter beam and returning during the intrinsic coherence lifetime (set by buffer gas collisions and diffusion to the cell walls). A theoretical model based on multiple return of atoms into the laser beam found good agreement with measured EIT spectra [71]. In general, the contrast of the narrow peak of the EIT spectrum decreases when buffer gas pressure is higher, laser power is higher, or the laser beam is larger. The sharp peak linewidth is mainly determined by the intrinsic coherence decay rate (i. e., it is not limited by the time to diffuse out of the laser beam on a single pass), and is relatively insensitive to power broadening.

The pointed EIT lineshape commonly exhibited in buffer gas cells poses a challenge for high-efficiency slow and stored light. To avoid large signal pulse absorption and reshaping, the bandwidth of the signal pulse should be significantly less than the sharp peak linewidth. However, the slow-light delay for such a pulse is often not long enough for high-efficiency light storage, because only a small part of the atoms contribute to the narrow peak, i. e., the effective optical depth for the useful sharp peak of the EIT spectrum is much smaller than the nominal optical depth. For instance, for the Ramsey-narrowed EIT experiments described in [72], a Gaussian waveform was employed for the signal pulse with a (relatively long) temporal length of 1 ms, which experienced a group delay of about 450 μs for a control field power of 50 μW. Note that a larger control field intensity was used at the retrieval (600 μW) to increase the EIT linewidth and thereby minimize losses during release and propagation of the retrieved signal pulse. The $1/e$ storage time was about 500 μs, corresponding to a decoherence rate consistent with the linewidth of the sharp peak of the EIT spectrum at low laser intensities, but much longer than the lowest order diffusive escape time calculated from Eq. (9). For the highest efficiency of stored light in buffer gas cells, it is desirable to use a laser beam diameter that is large enough to maximize the coherence lifetime, and also to have enough laser power to provide high EIT transmission and efficient readout. Given practical constraints on laser power, one must determine an optimal laser beam diameter to maximize light storage efficiency.

Firstenberg and coworkers carried out a comprehensive study of the effects on EIT of thermal atomic motion in buffer gas cells, including an assessment of the effect of misalignment of the control and signal fields (i. e., differing k vectors when these fields are not collinear) [73, 74]. They found that the EIT lineshape broadens and its contrast degrades as the angle between the control and signal fields increases, due to residual Doppler broadening of the two-photon EIT resonance [74]. Moreover, when a non-collimated beam such as a diffracted beam is considered, the signal field transmission becomes a function of position within the laser beam, similar to the intensity distribution in diffraction. This feature was utilized to eliminate and manip-

ulate effects of optical diffraction by adjusting the EIT two-photon detuning [75,76]. Similar effects were also exploited to slow and store images, of both the input light amplitude and phase, using EIT in warm-atom buffer gas cells [77,78]. In warm-atom buffer cells, diffusion of coherently prepared atoms is an issue that must be addressed in high-resolution and long-time image storage. A "phase shift" method [79] and storing of the image's Fourier plane [80,81] were proposed to offset the effects of diffusion; both proved effective.

4.3. Dual-structure EIT lineshapes in cells with anti-relaxation wall coatings

Coating the glass inner walls of an atomic vapor cell with an anti-relaxation layer such as paraffin is another way to prolong atomic coherence lifetimes by reducing the effects of atom-wall collisions on atomic hyperfine and Zeeman states. An EIT linewidth as narrow as 1 Hz has been realized in such paraffin-coated cells (no buffer gas) [34]; and recent improvements in coating materials have enabled coherence lifetimes as long as a minute [82,83]. Coated cells are actively being used for magnetometer [84], atomic clock [85], and quantum optics [86–88] applications. In comparison to buffer gas cells, coated cells do not suffer from collisional decoherence of excited states due to the buffer gas, which destroys quantum correlations in heralded photon generation experiments [89]. Thus, coated cells may be the best candidates for the use of warm vapor cells in single-photon experiments [87].

The typical EIT lineshape in a coated cell has a dual structure [86,90] (Fig. 12a). A narrow central peak results from multiple coherent atom-light interactions, as the atoms make many wall collisions before suffering decoherence. The linewidth of the narrow peak set by the intrinsic atomic coherence lifetime, which is determined by coating quality, cell geometry, magnetic field inhomogeneity, etc. A broad pedestal underlying the narrow peak arises from atom-light interactions during a one-time pass of atoms through the laser beam. Slow and stored light in coated cells can operate on two different time scales corresponding to signal pulses with spectral widths that fit within the linewidth of either the narrow peak or broad pedestal structures of the EIT lineshape. For instance, in [86], slow light in a coated cell was observed for signal pulse widths of both 5 ms and 50 µs. However, the fractional pulse delay was limited to only about 30%, due to radiation trapping, which prevents further increase of efficiency at higher optical depth. In general for coated cells, the stored light efficiency is low, although the storage time can be long ($\simeq$ 8 ms has been observed, see Fig. 12b [91]).

The low stored light efficiency is determined by fundamental issues associated with the ballistic motion of atoms in coated cells. For warm atoms, Zeeman EIT (ground states are degenerate Zeeman levels) has much lower contrast than for hyperfine EIT (ground states are non-degenerate hyperfine levels), because for Zeeman EIT the two-photon transition matrix elements have opposite signs for the two excited states (D1 line of ^{87}Rb, for example) which are partly mixed under Doppler broadening. Hence ground-state Zeeman coherence induced via EIT coupling through the two excited states will destructively interfere [92]. However, for hyperfine EIT to work in a coated cell, the atoms must not move beyond the range of the hyperfine wavelength, which is approximately 4 cm for ^{87}Rb. (Atoms with smaller hyperfine splitting and hence longer hyperfine wavelength are also being investigated to overcome such issues [93].) In addition, a high-intensity laser beam with diameter comparable to the size of the cell is desirable for efficient readout of all the stored coherence within the cell, which demands very high

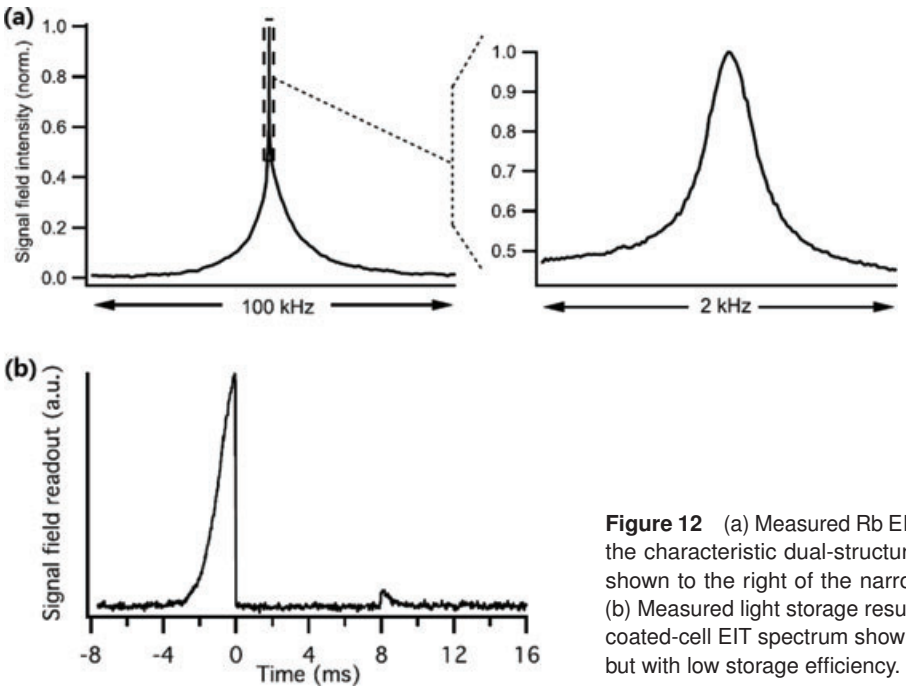

Figure 12 (a) Measured Rb EIT spectrum from a coated cell, exhibiting the characteristic dual-structure EIT lineshape. An expanded view is shown to the right of the narrow central feature of the EIT spectrum. (b) Measured light storage resulting from the narrow central peak of the coated-cell EIT spectrum shown in (a); 8 ms of storage time is realized, but with low storage efficiency. (Reproduced from [91].)

laser power for typical centimeter-diameter cells. Motivated by these constraints, a narrow diameter (1 mm) coated cell for Rb vapor was constructed to limit longitudinal atomic motion and enable the use of a brighter laser beam for readout. Initial hyperfine EIT and slow light results [94] show that the narrow cell geometry is promising, but requires improvement in the quality of the wall coating for optimal slow and stored light performance.

While the rapid atomic motion in coated cells has detrimental effects on light storage efficiency, it can be a useful feature for other applications. For instance, a recent demonstration of a slow light beam splitter [95] takes advantage of the rapid motion of atoms in a coated cell to spread coherence from one location to the entire cell, allowing the coherence to be converted back into light at a different location in the cell. Since atomic coherence is rapidly shared within a coated cell, light from different locations is phase coherent, as long as the cell is much smaller than the wavelength of the atomic ground-state coherence. The light splitting ratio provided by this technique is also adjustable by means of altering the laser power. With further improvements in atom-light state transfer efficiency, such a variable beam splitter may be used as an optical router for classical communications or a multiport programmable beam splitter for quantum repeater applications.

5. Storage of non-classical states

Following the proof-of-principle demonstrations of stored (classical) light using EIT in both warm- and cold-atom ensembles [7, 8, 96, 97], the focus of the EIT community turned to the storage of non-classical signal fields, with a leading motivation being the development of a practical quantum repeater using atomic ensembles. Great progress in this research program has been made over the last decade, as discussed in detail in several comprehensive review articles [13–15]. Here, we concentrate on issues and progress relevant to the storage of non-classical states using warm-atom EIT and related techniques.

Theoretically, there is only a modest difference between the EIT-based storage of a classical and quantum optical signal, although appropriate Langevin noise operators must be added to Eq. (1) to account for the effects of quantum fluctuations, following a well-established procedure [98–100]. However, while the simplified three-level approximation for atomic ensemble EIT works sufficiently well for mean-value calculations, a more comprehensive treatment of the energy level structure of real atoms (e. g., including all the hyperfine and Zeeman levels in both ground and excited states) is required for a realistic analysis of the effect of noise on the storage of quantum states [101]. In addition, inhomogeneous broadening of optical transitions can be significant in vapor cells, which can adversely affect the fidelity of quantum state storage due to atomic velocity-dependent variations in atom-light interactions [102, 103].

Experiments with quantum signals (either few-photon pulses or quasi-continuous squeezed vacuum pulses) are also much more technically challenging than with classical signals, since quantum states are more fragile and difficult to detect with high fidelity. In particular, since optical losses degrade quantum states to regular vacuum states, losses must be minimized for all system components, including interfaces between the signal field source, atomic vapor light storage cell, detector, etc. Also, nearly perfect transparency of the atomic ensemble under EIT conditions is required. However, in any realistic experiment there is residual absorption due to the finite lifetime of the dark state, e. g., as given by Eq. (4). This absorption increases at high optical depth, inhibiting realization of a quantum memory with high storage efficiency, as discussed in Sect. 3. Furthermore, the quantum efficiency must be high for the signal field detectors, which is a particularly severe requirement for single-photon measurements; although photon-counting detectors with high quantum efficiency have been recently demonstrated [104, 105], no suitable off-the-shelf devices are currently commercially available.

Another challenge is that the relatively narrow (up to a few megahertz) EIT linewidth provided by atomic ensembles limits the bandwidth of non-classical optical fields that can be slowed down and stored with high efficiency. Thus, such experiments require a source of resonant, narrow-band non-classical light to fit within the linewidth of the EIT window. Currently, the most common single-photon source is based on parametric down-conversion in nonlinear crystals [105]. However, the bandwidth of single photons produced with this technique is usually very broad (typically a few nanometers wide) due to the large spectral bandwidth of optical nonlinearity in crystals. Narrow-band powerful pump lasers and high-quality cavities permit narrowing the photon bandwidth to a few megahertz [106–108], but this is still a very challenging technical task.

Optical loss is not the only factor adversely affecting quantum state storage using EIT in warm atomic ensembles. The fidelity of quantum measurements is reduced if any additional optical fields are present in the mode of the desired non-classical signal field. The quality of a quantum signal is also degraded by incoherent fields generated as a result of atom-control field interactions. Recent experiments investigating squeezed vacuum generation in Rb vapor based on polarization self-rotation and associated quantum noise properties [109–115] demonstrated that spontaneous emission due to residual absorption of the control field can be strongly enhanced due to coupling back to the atomic transitions. It was also recently demonstrated that buffer-gas-induced collisional dephasing of the alkali metal excited electronic state, which is much stronger than for the ground state, results in additional unwanted *incoherent* Raman scattering [89], which produces photons at the optical transition frequency, rather than the Raman resonance frequency, and thus does not provide the photon-spin coupling that underlies all EIT effects. These spontaneous and incoherent Raman photons must be eliminated from the signal field detection channel either by spectral filtering, which adds further technical complication, or by reduction of the collision rate, e. g., by lowering the buffer gas pressure, which reduces the atom-light interaction time and thus degrades the quality of the EIT resonance.

In addition, it is essential to cleanly separate the signal and control fields at the detection stage after interaction with atomic ensembles. The closeness of the signal and control optical frequencies limits the utility of spectroscopic filtering methods, since traditional dispersive elements and interference filters cannot efficiently resolve two optical fields separated by only a few gigahertz. Application of spatial filtering is limited as well in a warm-atom system, since nearly collinear propagation of the signal and control fields is required to avoid large two-photon Doppler broadening, which occurs when $(\mathbf{k}_c - \mathbf{k}_s) \cdot \mathbf{v}_{atoms}$ becomes comparable to or larger than the ground-state linewidth. For example, an angle mismatch as small as 0.25 mrad between the signal and control fields produces about 100 kHz Doppler broadening for warm atoms. Such stringent requirement of collinearity of the signal and control fields makes spatial filtering inadequate for the necessary separation of the fields at the detection stage. To address this challenge, multiple spectral filtering stages have been required, such as optically pumped filtering cells and/or Fabry-Perot etalons [89, 116, 117].

5.1. Single-photon storage

Over the last decade, the prospects of practical realization of a quantum repeater based on atomic ensembles using the DLCZ protocol, proposed by Duan, Lukin, Cirac, and Zoller in 2001 [118], stimulated many research groups to investigate EIT-based interactions of single- or few-photon pulses with both warm and cold atomic ensembles. The DLCZ protocol produces entanglement between two distant atomic ensembles by probabilistic entanglement of pairs of neighboring ensembles followed by entanglement swapping between adjacent pairs to extend the created entanglement; the procedure is then repeated for a series of separated ensemble pairs to extend the entanglement to arbitrary distances. In the traditional realization of the DLCZ protocol, both ensembles in a pair separated by some distance L less than the absorption length of the photon communication channel are illuminated with an identical off-resonance classical pump field until a spontaneous Raman process occurs producing a single spin wave and emission of a correlated single Stokes photon in the forward direction. The photon outputs from both ensembles are directed to interfere on a beam splitter and measured with two sensitive photodetectors. It is important that the probability of Stokes emission is kept low to ensure no double excitations within one ensemble or simultaneous excitation in both ensembles. If only one Stokes photon is emitted, the click in one (and only one) of the two detectors indicates the creation of maximally entangled states between the two ensembles. If zero or more than one photons are detected, then the process must be repeated. After entanglement is successfully created within each of two adjacent ensemble pairs, with one ensemble in each entangled pair being in close proximity, the entanglement is extended to the two widely separated ensembles in the two pairs (separated by $2L$) by performing an entanglement swapping operation between the two co-located ensembles (one from each originally entangled pair). Such swapping is accomplished by illuminating the two co-located ensembles with a resonant classical control field that under EIT conditions converts the previously created spin excitation in each ensemble into an anti-Stokes photon. The photon outputs from the two co-located ensembles are then interfered on a beam splitter and measured. Since each emitted anti-Stokes photon is still entangled with the atomic spin excitation in the corresponding pair of originally entangled ensembles (each separated by distance L), a click in one (and only one) of the output photodetectors signifies entanglement creation between the two widely separated atomic ensembles in the two pairs. The same steps can be repeated to extend the entanglement even further over successive pairs of ensembles each separated by a distance L. The proposed protocol can be largely insensitive to many realistic losses, and predicts polynomial (rather than exponential) scaling of entanglement preparation time with distance. Further theoretical development of the original DLCZ protocol is reviewed in [119].

Experimental realization of the full DLCZ protocol or its variants has not yet been achieved, due to many technical challenges for both cold and warm atoms. Nevertheless, many essential steps for a DLCZ-type quantum repeater have been experimentally demonstrated, including quantum correlation and entanglement between the initial single-photon pulse emitted in the spontaneous Raman process and the later single-photon pulse retrieved under EIT conditions [116, 120–127]. In these demonstration experiments, much like the first part of the DLCZ protocol outlined above, the first (Stokes) photon is produced by spontaneous Raman generation under the action of a strong off-resonance laser field, which simultaneously creates a spin coherence in the atomic ensemble. This coherence is later read out by a resonant optical field under EIT and slow/stored light conditions, resulting in the generation of a second, correlated (anti-Stokes) photon. Quantum mechanical correlations between these two photons can be verified by measuring their photon-number fluctuations using a Hanbury-Brown-Twiss-type setup, which allows measurement of normalized correlation functions:

$$g^{(2)}(n_{AS}, n_S) = \frac{\langle : \hat{n}_{AS}, \hat{n}_S : \rangle}{\langle \hat{n}_{AS} \rangle \langle \hat{n}_S \rangle}, \qquad (11)$$

where $\hat{n}_{S,AS}$ denote the photon-number operators for the Stokes and anti-Stokes fields, correspondingly, and :: denotes operator normal ordering. For classical sources of light the value for the correlation function is $g^{(2)} = 1$, and for ideally correlated photons $g^{(2)} = 0$. A measured value of $g^{(2)} < 1$ indicates non-classical correlations between two photons. In practice, ideal correlation between two photons cannot be achieved due to optical losses, photodetector dark counts, contamination from spontaneous photons, etc. For example, if the overall Stokes photon detection efficiency is less than unity, it is possible to excite two or more independent spin excitations in the atomic ensemble even when only one Stokes photon is detected. Hence, any losses in the anti-Stokes channel reduce the observed correlations, since not every initial spin excitation

contributes to the final photon count. Thus, in warm-atom experiments to date [116, 124] the minimum observed value of $g^{(2)} = 0.3 \pm 0.2$ corresponded to the highest experimental photon detection efficiency and the lowest Raman scattering probability, which minimized the probability of scattering more than one Stokes photon. Including a buffer gas in a warm-atom vapor cell, to increase the light-atom interaction time, can create additional challenges: as discussed in Sect. 4, warm-atom diffusion in the presence of a buffer gas allows coherently prepared atoms to leave the optical interaction region, evolve in the dark, and re-enter the laser beam with a random phase, leading to emission of an anti-Stokes photon in a different spatial mode, and hence to reduced quantum correlations.

Despite such technical issues, photon-correlation experiments conducted in both warm and cold atomic ensembles, as well as demonstrations of entanglement between the Stokes photon and a spin excitation in an atomic ensemble [128–130], confirmed key aspects of the DLCZ protocol enabling demonstrations of entanglement of independent atomic ensembles [131–135].

Quantum repeaters and many other quantum optics and information applications require development of a long-lived quantum memory for few-photon pulses. Most existing demonstrations of single-photon storage and retrieval [19, 124, 136–139] used the generation of correlated photon pairs, described above, as a source of heralded single photons with controllable delay between the heralding (Stokes) and signal (anti-Stokes) pulses. With this technique the bandwidth of the emitted photons matches the EIT bandwidth in atomic ensembles used for storage; and the waveform of the generated few-photon pulses can still be modified with additional protocols [116, 125, 127, 140–142]. We note that EIT-based storage of single photons generated via parametric down-conversion has also been reported [143, 144].

To observe interaction of a single heralded anti-Stokes photon with a separate atomic ensemble under EIT and slow/stored light conditions, one can exploit the nonclassical intensity correlations between the Stokes and anti-Stokes photons and/or the conditional probability of anti-Stokes photon detection after appropriate delay from detection of the Stokes photon. Recent warm-atom experiments [124] demonstrated preservation of photon number correlations under EIT conditions for the initial Stokes photon and the anti-Stokes photon after its storage and retrieval in a separate atomic ensemble; these correlations then disappear when a two-photon detuning is introduced. For example, Fig. 13a illustrates the propagation of a single-photon anti-Stokes signal pulse under slow light conditions in a warm-atom vapor cell. The whole waveform is delayed after interaction with the atoms; this delay increases if the optical density is increased. In addition, as shown in Fig. 13b, a significant fraction of the single-photon anti-Stokes pulse can be stored in the target atomic ensemble and then recovered using EIT techniques.

The majority of EIT-based experiments relevant to the DLCZ protocol have been carried out using ^{87}Rb atoms, because of the availability of lasers resonant with relevant

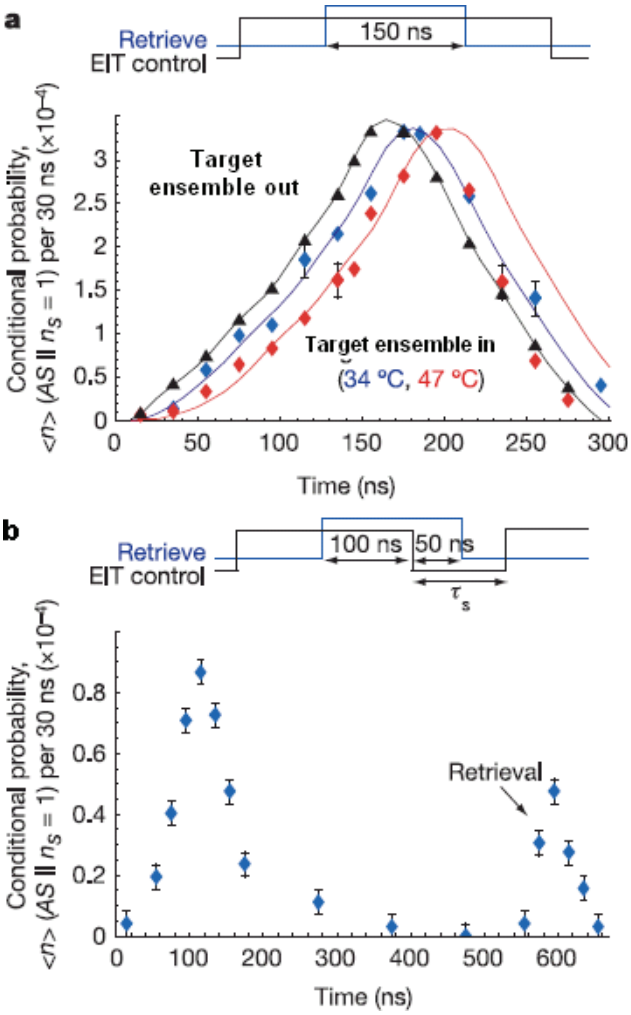

Figure 13 (online color at: www.lpr-journal.org) (a) Conditional probability (per 30 ns) of detecting an anti-Stokes photon transmitted through a target ensemble consisting of a 4.5-cm long Rb vapor cell with 8 torr of Ne buffer gas. Target ensemble absent (black triangles); target ensemble present at a temperature of 34.6 °C (blue diamonds) and 47 °C (red diamonds). Probability amplitude of delayed pulse at (34.6 °C, 47 °C) is scaled by (1.34, 2.14). Solid lines represent theoretical calculations for EIT propagation in a Doppler-broadened medium. (b) Storage and retrieval of a single-photon anti-Stokes pulse. EIT control is turned off 100 ns after the retrieval from the source ensemble begins; after waiting for a storage time of $\tau = 460$ ns, the EIT control is turned back on, resulting in the retrieved pulse centered at 600 ns. Target ensemble temperature of 47 °C. (Reproduced from [124].)

optical transitions, and the possibility of using the ^{85}Rb isotope as an absorption filter for the control field prior to single-photon detection. Recently, however, the storage of single-photon signal pulses has been demonstrated in Cs vapor [145]. In this experiment, a signal pulse with average photon number much less than one was produced by phase-modulation of the control field, following the method used for classical light storage. As discussed above, this method ensures phase coherence between the control and signal optical fields, and eliminates any residual Doppler

broadening due to imperfect collinear geometry between the control and signal fields. However, application of this technique at the single-photon level for signal pulses only became possible with the development of high-rejection bandpass optical filters based on a multi-pass Fabry-Perot etalon [117]. Such filters provide greater than 110 dB suppression of the unwanted control field without significant attenuation of the signal optical pulse.

Photon-based realizations of quantum information protocols require construction and manipulation of qubits. In particular, the EIT-based toolkit developed for realization of atom-photon correlations and entanglement, discussed above, can be directly applied to the storage of polarization qubits, in which information is encoded as a superposition of photon quantum states with orthogonal polarizations. In this case the two polarization modes of the original photon are spatially separated using a polarizing beam splitter, and then stored in two spatially separated atomic ensembles. After simultaneous retrieval, the two polarizations are recombined on the second beam splitter. Several cold-atom experiments have recently demonstrated such storage of polarization qubits with a lifetime of up to several milliseconds [21, 128, 137, 146]. While storage of a classical analogue of a polarization qubit in an atomic vapor cell has been performed [147], no warm-atom EIT-based quantum memory for a photonic polarization qubit has been reported yet.

5.2. Storage of squeezed light

There has also been great recent progress in the application of warm- and cold-atom EIT for the storage of continuous-variable quantum optical fields, such as squeezed light. For example, recent advances in periodically poled nonlinear crystals enabled the development of sources of narrow-band squeezed light or vacuum optical fields at wavelengths suitable for alkali metal optical transitions, e. g., using parametric down-conversion in periodically poled $KTiOPO_4$ crystals (PPKTP) [106–108]. The use of narrow-band powerful lasers, high-quality power build-up cavities, and sophisticated feedback electronics has also enabled dramatic reductions of technical noise at lower frequencies, and consequently allowed observation of optical squeezing at sideband frequencies below 100 kHz.

Key recent results include transmission of a squeezed vacuum field through an optically dense atomic ensemble under EIT conditions without complete loss of quantum noise suppression [148, 149]; controlled slow-light delay of squeezed vacuum pulses [150]; and storage of squeezed vacuum pulses achieved in both a Rb vapor cell [151, 152] and a cloud of laser-cooled Rb atoms [153]. Both of these storage experiments observed significant degradation of the optical field squeezing due to residual absorption of the input pulse by resonant atoms. Recently, these results were improved and extended to higher sideband frequencies by using a bichromatic control field to create a double EIT window tuned to both squeezed noise sidebands [154].

Note that an alternative, simpler method to generate resonant squeezed vacuum based on polarization self-rotation was first proposed in [109, 110], and then realized by several research groups [103, 111, 115, 155]. This method relies on modification of the noise properties of a vacuum (orthogonal) component of a linearly polarized field propagating through a near-resonant atomic medium. Light shifts of the Zeeman sublevels induce polarization rotation of elliptically polarized light, resulting in cross-phase modulation between the two orthogonal components of a linearly polarized field and in squeezing of one of the noise quadratures of the vacuum field. Experimentally measured squeezing (< 2 dB of noise suppression below the fundamental quantum limit) is significantly less than predicted theoretically due to excess noise caused by spontaneous emission and its interaction with optically pumped atoms. However, a related method of squeezing generation in a non-degenerate scheme has achieved 3.5 dB of noise suppression [156].

The EIT-based continuous-variable quantum memory can be potentially integrated with another atom-based storage technique exploiting far off-resonance Raman interactions [15, 157]. For example, a quantum state of a weak coherent signal pulse was mapped non-locally into the spin states of two ensembles of warm Cs atoms through quantum non-demolition experiments [158]. Recently, an improved storage protocol was used to store a distinctly non-classical optical field (two-mode squeezed light) with fidelity above the classical benchmark [159]. Since this particular quantum memory protocol requires a very long coherence lifetime, it was realized using paraffin-coated vapor cells for relatively narrow-band optical pulses in a well-defined single spatial and temporal mode. Furthermore, an alternative version of a far-detuned Raman interaction was demonstrated to allow storage of broad-band (> 1 GHz) optical signal pulses in a warm atomic ensemble [160, 161].

6. Comparison of EIT light storage in atomic ensembles with other techniques

To date, most EIT experiments on slow and stored light have been performed in ensembles of warm or cold alkali metal atoms, since their energy level structure allows reasonably good realizations of a three-level Λ system, which is the canonical system for EIT. Achieving similar effects in solid-state systems is attractive for practical applications, but faces severe scientific and technical challenges. In particular, while atoms in an ensemble under good environmental control are nearly perfectly identical and indistinguishable, optically active color centers embedded into a solid matrix (defects, donor atoms, vacancies, etc.) suffer from large variations in their properties due to nanoscale differences in their surroundings (strain in the crystal, neighboring defects, etc.), which can lead to broad, inhomogeneous spectral absorption and emission properties, rapid inhomogeneous dephasing, non-radiative decay processes, etc. In most cases, these non-ideal (i. e., non-atom-like) properties preclude the realization of EIT and slow/stored light. Nonetheless, certain classes of solid-state materials, such as doped yttrium orthosilicate crystals (Pr^{3+}:Y_2SiO_5 or Eu^{3+}:Y_2SiO_5), exhibit sufficiently atom-like spin and optical properties. For

example, the homogeneous lifetime of the ground-state spin coherence associated with the dopant ions in such crystals can extend to many seconds; and the electronic energy level structure and optical properties can be suitable for realizing EIT and slow/stored light [162]. As a consequence, ion-doped crystals have been used to demonstrate EIT-based storage of optical pulses for more than a second [163].

Progress with such solid-state systems has also stimulated development of alternative quantum memory protocols to overcome the narrow bandwidth requirements of EIT-based light storage. For example, the highest light storage memory efficiency achieved to date in any system employed a protocol based on controlled reversible inhomogeneous broadening (CRIB) [164]. This technique uses a modified photon echo in which the original broad-band signal pulse is absorbed by a controllable inhomogeneously broadened atomic ensemble, such that the bandwidth of the pulse matches the broadening of the transition. The inhomogeneous broadening is achieved by applying an external magnetic or electric field gradient; and the memory readout is realized by reversing the applied gradient. Although this technique was first proposed for atomic vapors [165], it is particularly well suited for doped solid-state crystals, such as those described above, due to their narrow homogeneously broadened optical lines. Initial proposals considered storage of signal pulses in optical coherences, with the storage time limited by the intrinsic lifetime of the optical transition. Later proposals, however, extended these ideas to transfer of the stored optical coherence into a long-lived spin coherence [166]. The CRIB protocol has been used to demonstrate the highest efficiency coherent optical memory achieved with any technique: 69% in Pr^{3+}:Y_2SiO_5 [167] and 87% in a Rb vapor cell [168]. The Rb vapor CRIB experiment also demonstrated storage and retrieval of a train of 20 optical pulses with 2% storage efficiency, reaching a delay-bandwidth product of 40. These parameters significantly surpass those demonstrated in EIT-based memories (for which the highest storage efficiency realized to date is approximately 43%, with a delay-bandwidth product of less than 1).

The atomic frequency comb (AFC) memory technique [169] employs an inhomogeneously broadened medium with a modulated optical absorption spectrum that consists of a series of evenly spaced narrow absorption peaks. Frequency components of a broad-band signal pulse are absorbed by the AFC and then re-emitted after a predetermined storage time [170]. The storage time can be extended in a controllable manner by transferring the optical excitation into a long-lived spin coherence and back by applying π-pulses [171]. The main advantages of the AFC memory are its intrinsic multimode storage capacity and favorable scaling with optical depth compared to other protocols [172–174].

Since many applications of slow and stored light are geared towards telecommunication applications and long-distance network development, it is important to realize these effects for light at wavelengths optimally suited for optical fiber transmission (1300 and 1550 nm). Researchers are working actively on this challenging task using a variety of protocols and systems. For example, a CRIB-based protocol has been used to store and retrieve weak coherent light pulses, including single photons, in an Er-doped Y_2SiO_5 crystal at cryogenic temperatures (2.6 K) [175]. Other recent experiments have demonstrated EIT in a quantum dot-based "artificial atom" [176, 177]. In addition, several groups have explored the slowing and storing of short optical pulses in specially designed photonic structures [178, 179], in which the role of the atomic ensemble is played by optical resonators with controllable coupling. Finally, EIT-like behavior has been predicted and demonstrated for surface electromagnetic fields (surface plasmon polaritons), localized in metal nanostructures [180, 181]. Dynamic control over the coupling between two types of nanostructures allows trapping of plasmons in a non-interacting mode, similar to a dark state in an atomic ensemble. We look forward to further continued progress in all the areas discussed above.

Acknowledgements. I. N. would like to acknowledge financial support from the National Science Foundation (grant no. PHY-0758010). Y. X. would like to acknowledge financial support from the Natural Science Foundation of China (grant nos. 10904018 and 61078013) and the Shanghai Pujiang Fund (grant no. 10PJ1401400).

Received: 25 March 2011, **Revised:** 7 June 2011, **Accepted:** 20 July 2011

Published online: 20 September 2011

Key words: Spin coherence, electromagnetically induced transparency, slow light, stored light, vapor cells, warm atoms.

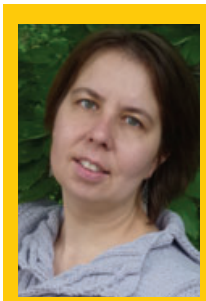

Irina Novikova has earned her undergraduate Diploma in physics from Moscow State Engineering-Physics Institute in 1998. She then continued her education by doing graduate studies at the Texas A & M University under the supervision of Prof. George R. Welch, and obtained a Ph. D. in experimental AMO physics in 2003. After spending three years as a postdoctoral fellow at the Harvard-Smithsonian Center for Astrophysics, in 2006 she joined the physics faculty at the College of William & Mary. Irina's research is focused on investigation of coherent light-atom interactions and their applications for quantum optics, precision metrology and telecommunications.

Ronald Walsworth is a Senior Lecturer on Physics at Harvard University and a Senior Physicist at the Smithsonian Astrophysical Observatory. He leads an interdisciplinary research group with a focus on developing precision measurement tools and applying them to important problems in both the physical and life sciences - from fundamental symmetry tests, astrophysics and quantum optics to nanoscience, neuroscience and bioimaging.

Yanhong Xiao obtained her Bachelors and Masters degree in Electronic Engineering from Tsinghua University, Beijing, China, in 1998 and 2000, respectively. In 2004, she received a Ph. D. degree in Applied Physics from Harvard University. Her Ph. D. research was on laser cooling of atoms. She then did postdoctoral research at Harvard-Smithsonian Center for Astrophysics, working on Electromagnetically Induced Transparency related experiments and their applications in quantum communication and atomic clocks. She joined the faculty of physics at Fudan University, Shanghai, China in 2009. Her research interests are to develop novel atomic spectroscopy techniques and to apply them in precision measurements, metrology and biology.

References

[1] M. O. Scully and M. S. Zubairy, Quantum Optics (Cambridge University Press, Cambridge, 1997).
[2] S. E. Harris, Phys. Today **50**, 36 (1997).
[3] L. V. Hau, S. E. Harris, Z. Dutton, and C. H. Behroozi, Nature **397**, 594 (1999).
[4] M. M. Kash, V. A. Sautenkov, A. S. Zibrov, L. Hollberg, G. R. Welch, M. D. Lukin, Y. Rostovtsev, E. S. Fry, and M. O. Scully, Phys. Rev. Lett. **82**, 5229 (1999).
[5] D. Budker, D. F. Kimball, S. M. Rochester, and V. V. Yashchuk, Phys. Rev. Lett. **83**, 1767 (1999).
[6] M. Fleischhauer and M. D. Lukin, Phys. Rev. Lett. **84**, 5094, (2000); Phys. Rev. A **65**, 022314 (2002).
[7] C. Liu, Z. Dutton, C. H. Behroozi, and L. V. Hau, Nature **409**, 490 (2001).
[8] D. F. Phillips, A. Fleischhauer, A. Mair, R. L. Walsworth, and M. D. Lukin, Phys. Rev. Lett. **86**, 783 (2001).
[9] A. V. Turukhin, V. S. Sudarhanam, M. S. Shahriar, J. A. Musser, B. S. Ham, and P. R. Hemmer, Phys. Rev. Lett. **88**, 023602 (2002).
[10] M. D. Lukin, Rev. Mod. Phys. **75**, 457 (2003).
[11] A. B. Matsko, O. Kocharovskaya, Y. Rostovtsev, G. R. Welch, A. S. Zibrov, and M. O. Scully, Adv. Atom. Mol. Opt. Phys. **46**, 191 (2001).
[12] M. Fleischhauer, A. Imamoglu, and J. P. Marangos, Rev. Mod. Phys. **77**, 633 (2005).
[13] H. J. Kimble, Nature **453**, 1023 (2008).
[14] A. I. Lvovsky, B. C. Sanders, and W. Tittel, Nature Photon. **3**, 706 (2009).
[15] K. Hammerer, A. S. Sorensen, and E. S. Polzik, Rev. Mod. Phys. **82**, 1041 (2010).
[16] C. Simon, M. Afzelius, J. Appel, A. Boyer de la Giroday, S. J. Dewhurst, N. Gisin, C. Y. Hu, and F. Jelezko, S. Kröll, J. H. Müller, J. Nunn, E. S. Polzik, J. G. Rarity, H. De Riedmatten, W. Rosenfeld, and A. J. Shields, N. Sköld, R. M. Stevenson, R. Thew, I. A. Walmsley, M. C. Weber, H. Weinfurter, J. Wrachtrup, and R. J. Young, Eur. Phys. J. D **58**, 1 (2010).
[17] M. Erhard and H. Helm, Phys. Rev. A **63**, 043813 (2001).
[18] K. S. Choi, H. Deng, J. Laurat, and H. J. Kimble, Nature **452**, 67 (2008).
[19] R. Zhao, Y. O. Dudin, S. D. Jenkins, C. J. Campbell, D. N. Matsukevich, T. A. B. Kennedy, and A. Kuzmich, Nature Phys. **5**, 100 (2009).
[20] B. Zhao, Y. A. Chen, X.-H. Bao, T. Strassel, C. S. Chuu, X.-M. Jin, J. Schmiedmayer, Z. S. Yuan, S. Chen, and J. W. Pan, Nature Phys. **5**, 95 (2009).
[21] H. Tanji, S. Ghosh, J. Simon, B. Bloom, and V. Vuletic, Phys. Rev. Lett. **103**, 043601 (2009).
[22] R. Zhang, S. R. Garner, and L. V. Hau, Phys. Rev. Lett. **103**, 233602 (2009).
[23] J. Vanier, Appl. Phys. B **81**, 421 (2005).
[24] V. Shah, S. Knappe, P. D. D. Schwindt, and J. Kitching, Nature Photon. **1**, 649 (2007).
[25] M. D. Lukin, M. Fleischhauer, A. S. Zibrov, H. G. Robinson, V. L. Velichansky, L. Hollberg, and M. O. Scully, Phys. Rev. Lett. **79**, 2959 (1997).
[26] Y. Xiao, Mod. Phys. Lett. B **23**, 661 (2009).
[27] W. Happer, Rev. Mod. Phys. **44**, 169 (1972).
[28] E. Arimondo, Phys. Rev. A **54**, 2216 (1996).
[29] S. Brandt, A. Nagel, R. Wynands, and D. Meschede, Phys. Rev. A **56**, R1063 (1997).
[30] M. A. Bouchiat and J. Brossel, Phys. Rev. **147**, 41 (1966).
[31] G. Singh, P. Dilavore, and C. O. Alley, Rev. Sci. Instrum. **43**, 1388 (1972).
[32] H. G. Robinson and C. E. Johnson, Appl. Phys. Lett. **40**, 771 (1982).
[33] D. F. Phillips, A. Boca, and R. L. Walsworth, http://cfa-www.harvard.edu/~dphil/work/coat.pdf.
[34] D. Budker, V. Yashchuk, and M. Zolotorev, Phys. Rev. Lett. **81**, 5788 (1998).
[35] D. Budker, L. Hollberg, D. F. Kimball, J. Kitching, S. Pustelny, and V. V. Yashchuk, Phys. Rev. A **71**, 012903 (2005).
[36] M. T. Graf, D. F. Kimball, S. M. Rochester, K. Kerner, C. Wong, D. Budker, E. B. Alexandrov, M. V. Balabas, and V. V. Yashchuk, Phys. Rev. A **72**, 023401 (2005).
[37] M. V. Balabas, T. Karaulanov, M. P. Ledbetter, and D. Budker, Phys. Rev. Lett. **105**, 070801 (2010).
[38] A. B. Matsko, I. Novikova, M. O. Scully, and G. R. Welch, Phys. Rev. Lett. **87**, 133601 (2001).
[39] A. B. Matsko, I. Novikova, and G. R. Welch, J. Mod. Opt. **49**, 367 (2002).
[40] M. Klein, Y. Xiao, A. V. Gorshkov, M. Hohensee, C. D. Leung, M. R. Browning, D. F. Phillips, I. Novikova, and R. L. Walsworth, Proc. SPIE **6904**, 69040C1 (2008).
[41] M. D. Lukin, P. R. Hemmer, M. Löffler, and M. O. Scully, Phys. Rev. Lett. **81**, 2675 (1998).
[42] M. D. Lukin, A. B. Matsko, M. Fleischhauer, and M. O. Scully, Phys. Rev. Lett **82**, 1847 (1999).
[43] H. Kang, G. Hernandez, and Y. Zhu, Phys. Rev. A **70**, 061804 (2004).
[44] V. Wong, R. S. Bennink, A. M. Marino, R. W. Boyd, C. R. Stroud, and F. A. Narducci, Phys. Rev. A **70**, 053811 (2004).
[45] K. Harada, T. Kanbashi, M. Mitsunaga, and K. Motomura, Phys. Rev. A **73**, 013807 (2006).
[46] G. S. Agarwal, T. N. Dey, and D. J. Gauthier, Phys. Rev. A **74**, 043805 (2006).
[47] T. Tong, A. V. Gorshkov, D. Patterson, A. S. Zibrov, J. M. Doyle, M. D. Lukin, and M. G. Prentiss, Phys. Rev. A **79**, 013806 (2009).
[48] N. B. Phillips, A. V. Gorshkov, and I. Novikova, J. Mod. Opt. **56**, 1916 (2009).

[49] N. B. Phillips, A. V. Gorshkov, and I. Novikova, Phys. Rev. A **78**, 023801 (2008).
[50] R. M. Camacho, P. K. Vudyasetu, and J. C. Howell, Nature Photon. **3**, 103 (2009).
[51] N. B. Phillips, A. V. Gorshkov, and I. Novikova, Phys. Rev. A **83**, 063823 (2011).
[52] V. Boyer, C. F. McCormick, E. Arimondo, and P. D. Lett, Phys. Rev. Lett. **99**, 143601 (2007).
[53] C. F. McCormick, A. M. Marino, V. Boyer, and P. D. Lett, Phys. Rev. A **78**, 043816 (2008).
[54] V. Boyer, A. M. Marino, and P. D. Lett, Phys. Rev. Lett. **100**, 143601 (2008).
[55] A. V. Gorshkov, A. André, and M. Fleischhauer, A. S. Sørensen, and M. D. Lukin, Phys. Rev. Lett. **98**, 123601 (2007).
[56] I. Novikova, A. V. Gorshkov, and D. F. Phillips, A. S. Sørensen, M. D. Lukin, and R. L. Walsworth, Phys. Rev. Lett. **98**, 243602 (2007).
[57] A. V. Gorshkov, A. André, M. D. Lukin, and A. S. Sørensen, Phys. Rev. A **76**, 033804 (2007).
[58] A. V. Gorshkov, A. André, M. D. Lukin, and A. S. Sørensen, Phys. Rev. A **76**, 033805 (2007).
[59] A. V. Gorshkov, A. André, M. D. Lukin, and A. S. Sørensen, Phys. Rev. A **76**, 033806 (2007).
[60] A. V. Gorshkov, T. Calarco, and M. D. Lukin, and A. S. Sørensen, Phys. Rev. A **77**, 043806 (2008).
[61] I. Novikova, A. V. Gorshkov, D. F. Phillips, Y. Xiao, M. Klein, and R. L. Walsworth, Proc. SPIE **6482**, 64820M-1 (2007).
[62] I. Novikova, N. B. Phillips, and A. V. Gorshkov, Phys. Rev. A **78**, 021802(R) (2008).
[63] R. S. Tucker, P. S. Ku, and C. J. Chang-Hasnain, J. Lightwave Technol. **23**, 4046 (2005).
[64] J. Simon, H. Tanji, and J. K. Thompson, and V. Vuletić, Phys. Rev. Lett. **98**, 183601 (2007).
[65] M. Klein, M. Hohensee, Y. Xiao, R. Kalra, D. F. Phillips, and R. L. Walsworth, Phys. Rev. A **79**, 053833 (2009).
[66] F. Levi, A. Godone, J. Vanier, S. Micalizio, and G. Modugno, Eur. Phys. J. D **12**, 53 (2000).
[67] A. V. Taichenachev, A. M. Tumaikin, V. I. Yudin, M. Stahler, R. Wynands, J. Kitching, and L. Hollberg, Phys. Rev. A **69**, 024501 (2004).
[68] M. Klein, Y. Xiao, M. Hohensee, D. F. Phillips, and R. L. Walsworth, arXiv:0812.4939 (2009).
[69] R. H. Dicke, Phys. Rev. **89**, 472 (1953).
[70] Y. Xiao, I. Novikova, D. F. Phillips, and R. L. Walsworth, Phys. Rev. Lett. **96**, 043601 (2006).
[71] Y. Xiao, I. Novikova, D. F. Phillips, and R. L. Walsworth, Opt. Express **16**, 14128 (2008).
[72] I. Novikova, Y. Xiao, D. F. Phillips, and R. L. Walsworth, J. Mod. Opt. **52**, 2381 (2005).
[73] O. Firstenberg, M. Shuker, R. Pugatch, D. R. Fredkin, N. Davidson, and A. Ron, Phys. Rev. A **77**, 043830 (2008).
[74] M. Shuker, O. Firstenberg, R. Pugatch, A. Ben-Kish, A. Ron, and N. Davidson, Phys. Rev. A **76**, 023813 (2007).
[75] O. Firstenberg, M. Shuker, N. Davidson, and A. Ron, Phys. Rev. Lett. **102**, 043601 (2009).
[76] O. Firstenberg, P. London, M. Shuker, A. Ron, and N. Davidson, Nature Phys. **5**, 665 (2009).
[77] R. Pugatch, M. Shuker, O. Firstenberg, A. Ron, and N. Davidson, Phys. Rev. Lett. **98**, 203601 (2007).
[78] R. M. Camacho, C. J. Broadbent, I. Ali-Khan, and J. C. Howell, Phys. Rev. Lett. **98**, 043902 (2007).
[79] M. Shuker, O. Firstenberg, R. Pugatch, A. Ron, and N. Davidson, Phys. Rev. Lett. **100**, 223601 (2008).
[80] L. Zhao, T. Wang, Y. Xiao, and S. F. Yelin, Phys. Rev. A **77**, 041802 (2008).
[81] P. K. Vudyasetu, R. M. Camacho, and J. C. Howell, Phys. Rev. Lett. **100**, 123903 (2008).
[82] M. V. Balabas, T. Karaulanov, M. P. Ledbetter, and D. Budker, Phys. Rev. Lett. **105**, 070801 (2010).
[83] M. V. Balabas, K. Jensen, W. Wasilewski, H. Krauter, L. S. Madsen, J. H. Muller, T. Fernholz, and E. S. Polzik, Opt. Express **18**, 5825 (2010).
[84] M. V. Balabas, D. Budker, J. Kitching, P. D. D. Schwindt, and J. E. Stalnaker, J. Opt. Soc. Am. B **23**, 1001 (2006).
[85] H. G. Robinson and C. E. Johnson, IEEE Trans. Instrum. Meas. **32**, 198 (1983).
[86] M. Klein, I. Novikova, D. F. Phillips, and R. L. Walsworth, J. Mod. Opt. **53**, 2583 (2006).
[87] S. Jiang, X. M. Luo, L. Q. Chen, B. Ning, S. Chen, J. Wang, Z. Zhong, and J.-W. Pan, Phys. Rev. A **80**, 062303 (2009).
[88] J. Sherson, H. Krauter, R. K. Olsson, B. Julsgaard, and E. S. Polzik, J. Phys. B **41**, 223001 (2008).
[89] S. Manz, T. Fernholz, J. Schmiedmayer, and J.-W. Pan, Phys. Rev. A **75**, 040101(R) (2007).
[90] M. Klein, M. Hohensee, D. F. Phillips, and R. L. Walsworth, Phys. Rev. A **83**, 013826 (2011).
[91] M. Klein, PhD thesis, Harvard University (2009).
[92] I. Novikova, A. B. Matsko, and G. R. Welch, J. Opt. Soc. Am. B **22**, 44 (2005).
[93] J. S. Guzman, A. Wojciechowski, J. E. Stalnaker, K. Tsigutkin, V. V. Yashchuk, and D. Budker, Phys. Rev. A **74**, 053415 (2006).
[94] M. Klein, M. Hohensee, A. Nemiroski, Y. Xiao, D. F. Phillips, and R. L. Walsworth, App. Phys. Lett. **95**, 091102 (2009).
[95] Y. Xiao, M. Klein, M. Hohensee, L. Jiang, D. F. Phillips, M. D. Lukin, and R. L. Walsworth, Phys. Rev. Lett. **101**, 043601 (2008).
[96] A. B. Matsko, Y. V. Rostovtsev, O. Kocharovskaya, A. S. Zibrov, and M. O. Scully, Phys. Rev. A **64**, 043809 (2001).
[97] A. Mair, J. Hager, D. F. Phillips, R. L. Walsworth, and M. D. Lukin, Phys. Rev. A **65**, 031802(R) (2002).
[98] A. Dantan and M. Pinard, Phys. Rev. A **69**, 043810 (2004).
[99] A. Dantan, A. Bramati, and M. Pinard, Phys. Rev. A **71**, 043801 (2005).
[100] A. Dantan, J. Cviklinski, M. Pinard, and Ph. Grangier, Phys. Rev. A **73**, 032338 (2006).
[101] M. T. Hsu, G. Hétet, O. Glöckl, J. J. Longdell, B. C. Buchler, H.-A. Bachor, and P. K. Lam, Phys. Rev. Lett. **97**, 183601 (2006).
[102] P. Barberis-Blostein and M. Bienart, Phys. Rev. A **79**, 063824 (2009).
[103] E. E. Mikhailov, A. Lezama, T. W. Noel, and I. Novikova, J. Mod. Opt. **56** 1985 (2009).
[104] A. E. Lita, A. J. Miller, and S. W. Nam, Opt. Express **16**, 3032 (2008).
[105] R. H. Hadfield, Nature Photon. **3**, 697 (2009).
[106] G. Hétet, O. Glöckl, K. A. Pilypas, C. C. Harb, B. C. Buchler, H.-A. Bachor, and P. K. Lam, J. Phys. B **40**, 221 (2007).
[107] Y. Takeno, M. Yukawa, H. Yonezawa, and A. Furusawa, Opt. Express **15**, 4321 (2007).
[108] S. Burks, J. Ortalo, A. Chiummo, X. Jia, F. Villa, A. Bramati, J. Laurat, and E. Giacobino, Opt. Express **17**, 3777 (2009).

[109] A. B. Matsko, I. Novikova, G. R. Welch, D. Budker, D. F. Kimball, and S. M. Rochester, Phys. Rev. A **66**, 043815 (2002).
[110] I. Novikova, A. B. Matsko, and G. R. Welch, J. Mod. Opt. **49**, 2565 (2002).
[111] J. Ries, B. Brezger, and A. I. Lvovsky, Phys. Rev. A **68**, 025801 (2003).
[112] S. A. Zibrov, V. L. Velichansky, A. S. Zibrov, A. V. Taichenachev, and V. I. Yudin, JETP Lett. **82**, 477 (2005).
[113] M. T. L. Hsu, G. Hétet, A. Peng, C. C. Harb, H.-A. Bachor, M. T. Johnsson, J. J. Hope, P. K. Lam, A. Dantan, J. Cviklinski, A. Bramati, and M. Pinard, Phys. Rev. A **73**, 023806 (2006).
[114] A. Lezama, P. Valente, H. Failache, M. Martinelli, and P. Nussenzveig, Phys. Rev. A **77**, 013806 (2007).
[115] E. E. Mikhailov and I. Novikova, Opt. Lett. **33** 1213 (2008).
[116] M. D. Eisaman, L. Childress, A. André, F. Massou, A. S. Zibrov, and M. D. Lukin, Phys. Rev. Lett. **93**, 233602 (2004).
[117] D. Höckel, E. Martin, and O. Benson, Rev. Sci. Instrum. **81**, 026108 (2010).
[118] L. M. Duan, M. D. Lukin, J. I. Cirac, and P. Zoller, Nature **414**, 413 (2001).
[119] N. Sangouard, C. Simon, H. de Riedmatten, and N. Gisin, Rev. Mod. Phys. **83**, 33 (2011).
[120] C. H. van der Wal, M. D. Eisaman, A. Andre, R. L. Walsworth, D. F. Phillips, A. S. Zibrov, and M. D. Lukin, Science **301**, 196 (2003).
[121] C. W. Chou, S. V. Polyakov, A. Kuzmich, and H. J. Kimble, Phys. Rev. Lett. **92**, 213601 (2004).
[122] A. Kuzmich, W. P. Bowen, A. D. Boozer, A. Boca, C. W. Chou, L. M. Duan, and H. J. Kimble, Nature **423**, 731 (2003).
[123] S. V. Polyakov, C. W. Chou, D. Felinto, and H. J. Kimble, Phys. Rev. Lett. **93**, 263601 (2004).
[124] M. D. Eisaman, A. André, F. Massou, M. Fleischhauer, A. S. Zibrov, and M. D. Lukin, Nature **438**, 837 (2005).
[125] V. Balic, D. A. Braje, P. Kolchin, G. Y. Yin, and S. E. Harris, Phys. Rev. Lett. **94**, 183601 (2005).
[126] D. N. Matsukevich, T. Chaneliere, S. D. Jenkins, S. Y. Lan, T. A. B. Kennedy, and A. Kuzmich, Phys. Rev. Lett. **97**, 013601 (2006).
[127] S. W. Du, P. Kolchin, C. Belthangady, G. Y. Yin, and S. E. Harris, Phys. Rev. Lett. **100**, 183603 (2008).
[128] D. N. Matsukevich and A. Kuzmich, Science **306**, 663 (2004).
[129] D. N. Matsukevich, T. Chaneliere, M. Bhattacharya, S. Y. Lan, S. D. Jenkins, T. A. B. Kennedy, and A. Kuzmich, Phys. Rev. Lett. **95**, 040405 (2005).
[130] Y. O. Dudin, S. D. Jenkins, R. Zhao, D. N. Matsukevich, A. Kuzmich, and T. A. B. Kennedy, Phys. Rev. Lett. **103**, 020505 (2009).
[131] C. W. Chou, H. De Riedmatten, S. V. Polyakov, S. J. van Enk, and H. J. Kimble, Nature **438**, 828 (2005).
[132] D. Matsukevich, T. Chanelière, S. D. Jenkins, T. A. B. Kennedy, M. S. Chapman, and A. Kuzmich, Phys. Rev. Lett. **96**, 030405 (2006).
[133] D. Felinto, C. W. Chou, J. Laurat, E. W. Schomburg, H. De Riedmatten, and H. J. Kimble, Nature Phys. **2**, 844 (2006).
[134] C. W. Chou, J. Laurat, H. Deng, K. S. Choi, H. de Riedmatten, D. Felinto, and H. J. Kimble, Science **316**, 1316 (2007).
[135] J. Laurat, K. S. Choi, H. Deng, C. W. Chou, and H. J. Kimble, Phys. Rev. Lett. **99**, 180504 (2007).
[136] T. Chanelière, D. Matsukevich, S. D. Jenkins, S.-Y. Lan, T. A. B. Kennedy, and A. Kuzmich, Nature **438**, 833 (2005).
[137] K. S. Choi, H. Deng, J. Laurat, and H. J. Kimble, Nature **452**, 67 (2008).
[138] S. Y. Lan, A. G. Radnaev, O. A. Collins, D. N. Matsukevich, T. A. B. Kennedy, and A. Kuzmich, Opt. Express **17**, 13639 (2009).
[139] A. G. Radnaev, Y. O. Dudin, R. Zhao, H. H. Jen, S. D. Jenkins, A. Kuzmich, and T. A. B. Kennedy, Nature Phys. **6**, 894 (2010).
[140] P. Kolchin, C. Belthangady, S. W. Du, G. Y. Yin, and S. E. Harris, Phys. Rev. Lett. **101**, 103601 (2008).
[141] S. Sensarn, G. Y. Yin, and S. E. Harris, Phys. Rev. Lett. **103**, 163601 (2009).
[142] S. Sensarn, G. Y. Yin, and S. E. Harris, Phys. Rev. Lett. **104**, 253602 (2010).
[143] K. Akiba, K. Kashiwagi, T. Yonehara, and M. Kozuma, Phys. Rev. A **76**, 023812 (2007).
[144] K. Akiba, K. Kashiwagi, M. Arikawa, and M. Kozuma, New J. Phys. **11**, 013049 (2009).
[145] D. Höckel, and O. Benson, Phys. Rev. Lett. **105**, 153605 (2010).
[146] Y. O. Dudin, A. G. Radnaev, R. Zhao, J. Z. Blumoff, T. A. B. Kennedy, and A. Kuzmich, Phys. Rev. Lett. **105**, 260502 (2010).
[147] Y.-W. Cho and Y.-H. Kim, Opt. Express **18**, 25786 (2010).
[148] D. Akamatsu, K. Akiba, and M. Kozuma, Phys. Rev. Lett. **92**, 203602 (2004).
[149] M. Arikawa, K. Honda, D. Akamatsu, Y. Yokoi, K. Akiba, S. Nagatsuka, A. Furusawa, and M. Kozuma, Opt. Express **15**, 11849 (2007).
[150] D. Akamatsu, Y. Yokoi, M. Arikawa, S. Nagatsuka, T. Tanimura, A. Furusawa, and M. Kozuma, Phys. Rev. Lett. **99**, 153602 (2007).
[151] J. Appel, E. Figueroa, D. Korystov, and A. I. Lvovsky, Phys. Rev. Lett. **100**, 093602 (2008).
[152] E. Figueroa, M. Lobino, D. Korystov, J. Appel, and A. I. Lvovsky, New J. Phys. **11**, 013044 (2009).
[153] K. Honda, D. Akamatsu, M. Arikawa, Y. Yokoi, K. Akiba, S. Nagatsuka, T. Tanimura, A. Furusawa, and M. Kozuma, Phys. Rev. Lett. **100**, 093601 (2008).
[154] M. Arikawa, K. Honda, D. Akamatsu, S. Nagatsuka, K. Akiba, A. Furusawa, and M. Kozuma, Phys. Rev. A **81**, 021605(R) (2010).
[155] I. H. Agha, G. Messin, and P. Grangier, Opt. Express **18**, 4198 (2010).
[156] W. Wasilewski, T. Fernholz, K. Jensen, L. S. Madsen, H. Krauter, C. Muschik, and E. S. Polzik, Opt. Express **17**, 14444 (2009).
[157] A. E. Kozhekin, K. Mølmer, and E. Polzik, Phys. Rev. A **62**, 033809 (2000).
[158] B. Julsgaard, J. Sherson, J. Fiurasek, I. Cirac, and E. S. Polzik, Nature **432**, 482 (2004).
[159] K. Jensen, W. Wasilewski, H. Krauter, T. Fernholz, B. M. Nielsen, M. Owari, M. B. Plenio, A. Serafini, M. M. Wolf, and E. S. Polzik, Nature Phys. **7**, 13 (2011).
[160] J. Nunn, I. A. Walmsley, M. G. Raymer, K. Surmacz, F. C. Waldermann, Z. Wang, and D. Jaksch, Phys. Rev. A **75**, 011401(R) (2007).

[161] K. F. Reim, J. Nunn, V. O. Lorenz, B. J. Sussman, K. C. Lee, N. K. Langford, D. Jaksch, and I. A. Walmsley, Nature Photon. **4**, 218 (2010).
[162] A. V. Turukhin, V. S. Sudarshanam, and M. S. Shahriar, J. A. Musser, B. S. Ham, and P. R. Hemmer, Phys. Rev. Lett. **88**, 023602 (2001).
[163] J. J. Longdell, E. Fraval, M. J. Sellars, and N. B. Manson, Phys. Rev. Lett. **95**, 063601 (2005).
[164] W. Tittel and M. Afzelius, T. Chaneliére, R. L. Cone, S. Kröll, S. Moiseev, and M. Sellars, Laser Photon. Rev. **4**, 244 (2010).
[165] S. A. Moiseev and S. Kroll, Phys. Rev. Lett. **87**, 173601 (2001).
[166] B. Kraus, W. Tittel, N. Gisin, and M. Nilsson, S. Kröll, and J. I. Cirac, Phys. Rev. A **73**, 020302 (2006).
[167] M. P. Hedges, J. J. Longdell, Y. Li, and M. J. Sellars, Nature **465**, 1052 (2010).
[168] M. Hosseini, B. M. Sparkes, P. K. Lam, and B. C. Buchler, Nature Commun. **2**, 174 (2011).
[169] M. Afzelius, C. Simon, H. de Riedmatten, and N. Gisin, Phys. Rev. A **79**, 052329 (2009).
[170] H. de Riedmatten, M. Afzelius, M. U. Staudt, C. Simon, and N. Gisin, Nature **456**, 773 (2008).
[171] M. Afzelius, I. Usmani, A. Amari, B. Lauritzen, A. Walther, C. Simon, and N. Sangouard, J. Minář, H. de Riedmatten, and N. Gizin, and S. Kröll, Phys. Rev. Lett. **104**, 040503 (2010).
[172] M. Bonarota and J. Ruggiero, J.-L. Le Gouët, and T. Chanelière, Phys. Rev. A **81**, 033803 (2010).
[173] I. Usmani, M. Afzelius, H. de Riedmatten, and N. Gizin, Nature Commun. **1**, 1 (2010).
[174] M. Sabooni, F. Beaudoin, A. Walther, N. Lin, A. Amari, and M. Huang, and S. Kröll, Phys. Rev. Lett. **105**, 060501 (2010).
[175] B. Lauritzen, J. Minář, H. de Riedmatten, M. Afzelius, N. Sangouard, C. Simon, and N. Gisin, Phys. Rev. Lett. **104**, 080502 (2010).
[176] A. A. Abdumalikov, O. Astafiev, A. M. Zagoskin, Y. A. Pashkin, Y. Nakamura, and J. S. Tsai, Phys. Rev. Lett. **104**, 193601 (2010).
[177] W. R. Kelly, Z. Dutton, J. Schlafer, B. Mookerji, T. A. Ohki, J. S. Kline, and D. P. Pappas, Phys. Rev. Lett **104**, 163601 (2010).
[178] M. F. Yanik, W. Suh, Z. Wang, and S. Fan, Phys. Rev. Lett. **93**, 233903 (2004).
[179] Q. Xu, P. Dong, and M. Lipson, Nature Phys. **3**, 406 (2007).
[180] S. Zhang, D. A. Genov, Y. Wang, M. Liu, and X. Zhang, Phys. Rev. Lett. **101**, 047401 (2008).
[181] N. Liu, L. Langguth, and T. Weiss, J. Kästel, M. Fleischhauer, T. Pfau, and H. Giessen, Nature Mater. **8**, 758 (2009).